Mining of Mineral Deposits
Volume 17 (2023), Issue 2, 121-139

MMD JOURNAL / MINING.IN.UA

https://doi.org/10.33271/mining17.02.121

Petrophysical analysis and hydrocarbon potential of the Matulla Formation in the Muzhil Field, central part of the Gulf of Suez, Egypt

Ahmed S. Mohamed[1*]✉, Awad A. Omran[2]✉, Mostafa T. Mohamed[2]✉, Bassem S. Nabawy[3]✉

[1] *Al-Azhar University, Qena, Egypt*
[2] *Assiut University, Assiut, Egypt*
[3] *National Research Center, Cairo, Egypt*

**Corresponding author: e-mail Ahmedsayed8686@yahoo.com*

Abstract

Purpose. The research is aimed at evaluating the petrophysical characteristics of the Late Cretaceous Matulla Formation in the central part of the Gulf of Suez in order to detect its hydrocarbon reservoir potential.

Methods. Well logs from five wells (Muzhil-1, -2, -4, -7, -8) were used to evaluate the Matulla reservoirs based on a computerized approach. Petrophysical parameters and fluid types were calculated, verified using core data, and represented vertically as lithosaturation cross plots and laterally as isoparametric variation maps.

Findings. Evaluation of total porosity (Φ_t), effective porosity (Φ_e), shale content (V_{sh}), water saturation (S_w), permeability (K), bulk volume of water (BVW), and net pay characteristics of Matulla Formation in the Muzhil wells showed the following weighted average values: 18-23%, 15-19%, 21-40%, 20-100%, 1.1-281 mD, 3-21% and 0-83 ft, respectively. The Log-derived lithology identification indicates that the major matrix component of the Matulla Formation is quartzose sandstone with minor shale and carbonate contents. The upper zone is a poor reservoir, while the middle and lower zones are considered good reservoirs in all studied wells. It is expected that Muzhil-2 will produce oil without water; however, Muzhil-1 and Muzhil-4 will produce oil with water; while Muzhil-7 and Muzhil-8 will produce water only.

Originality. Detailed log-derived petrophysical evaluation, verified by core analysis and well tests (DST and MDT), construction of lithosaturation cross plots for each well and isoparametric petrophysical maps are performed for the first time for Matulla Formation in the Muzhil field.

Practical implications. The obtained results on lithosaturation and petrophysics have expanded the knowledge about the characteristics of the Matulla Formation sediments, hosting promising reservoir intervals, and should be taken into account in future exploration and development of the Muzhil field.

Keywords: *hydrocarbon potentiality, well logging, formation evaluation, petrophysical parameters, Matulla Formation, Muzhil Field, Gulf of Suez*

1. Introduction

The Gulf of Suez (GOS) is one of the most important productive oil producing provinces in North Africa and the Middle East. The Matulla Formation is of great interest due to its contribution to the petroleum system in the GOS region. The Matulla Formation in the southern, central and eastern parts of the GOS and on the western side of Sinai can be considered as a good reservoir consisting of ferruginous sandstone inter-beds with good to excellent porosity, very good to excellent permeability and poor to fair flow zone indicator [1]-[13]. The Coniacian–Santonian deposits of the Matulla Formation are part of the Nezzazat Group, and they are distinguished by various lithologies, lateral facies and thickness changes, as well as reservoir heterogeneity throughout the GOS basin [9], [14]-[16]. Several authors have studied these deposits in terms of sedimentology, paleontology, depositional settings and structural settings [5], [9], [10], [17], [31].

However, their petrophysical characteristics are still poorly studied. The petrophysical characterization of reservoir rocks is a very challenging task in petroleum science, due to the wide variability in the properties of the host rocks [32], [33].

In this work the following are highlighted:

1) determining different petrophysical properties from well logging data of the Matulla Formation;

2) distribution of petrophysical properties vertically through the investigated succession in each well and horizontally through the Muzhil Field;

3) defining reservoir potential zones of Matulla Formation for hydrocarbon production.

The innovations of the present work are:

Received: 29 April 2023. Accepted: 23 June 2023. Available online: 30 June 2023

Mining of Mineral Deposits. ISSN 2415-3443 (Online) | ISSN 2415-3435 (Print)

1) to present detailed petrophysical characteristics of the Matulla Formation in Muzhil Field, which is still poorly studied;

2) to distinguish shale types and distribution, which tend to significantly influence the effective porosity and permeability of reservoirs;

3) to define how the petrophysical parameters have been greatly controlled the sedimentary lithofacies and diagenetic process.

Consequently, a complete lithology and petrophysical evaluation of the Matulla Formation in the eastern part of the Muzhil Field at the central Gulf of Suez was carried out using well log data from five wells (Muzhil-1, Muzhil-2, Muzhil-4, Muzhil-7 and Muzhil-8) approved by the Egyptian General Petroleum Corporation (EGPC) and South Abu Zienima Company (SAZ) in order to examine promising targets for the hydrocarbon reservoirs.

2. Study area

2.1. Location of the study area

The studied area is located in the offshore central part of the GOS between longitudes: 33°7′24″ E and 33°8′24″ E and latitudes: 28°53′12″ N and 28°54′47″ N comprising the eastern part of Muzhil field concession which covers an area of almost 150 km^2 (Fig. 1).

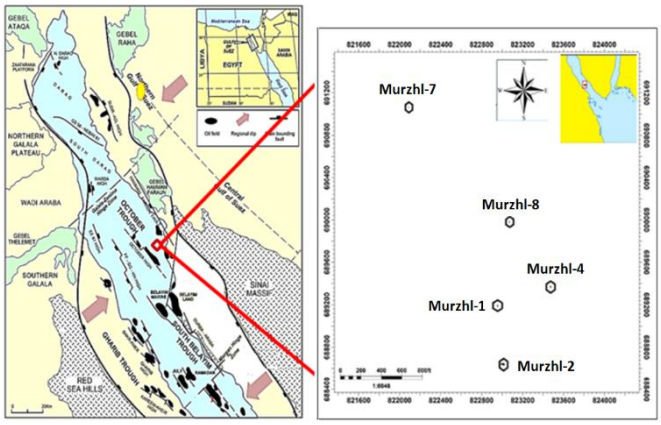

Figure 1. Location map of the Gulf of Suez, Abu Zenima Concession and the studied wells in Muzhil field area

2.2. Stratigraphy of the Gulf of Suez

The GOS width ranges from 30 to 50 km in the central part, and its length from the north tip at Suez City to the south tip at the Sinai Peninsula is approximately350 km. The water covers approximately25000 km^2 of the GOS rift basin with 55 m average water depth [6], [10], [34], [35]. The GOS started during the Late Oligocene, in synchronism with rifting of the Red Sea basin to the south. However, many studies have shown that extensional faulting commenced in the southern part of the Gulf and the rift probably propagated toward the north, intersecting with the east-west Suez city structural boundary, in the late Eocene age [36]. Figure 2 presents a generalized stratigraphic column for the GOS from the Pre-Cambrian to Recent [37].

Three depositional phases are generally assumed for the GOS stratigraphy [4], [7], [38]:

1. Devonian to Eocene sediments, which are typically limestone sand deposits, form the most important sand reservoirs in the GOS including Nubia sand, and other minor source rocks.

2. Lower Miocene sediments creating the GOS primary source rocks, some reservoirs, and sealing rocks.

3. Upper Miocene and Pliocene sediments are characterized by relatively younger deposits, which have a recent depositional history of the GOS graben.

The sedimentary sequence in the GOS can be divided into three stages according to the tectonic history of the Red Sea rift: the pre-rift, the syn-rift, and the post-rift stages [39].

2.3. Structure of the GOS rift

The GOS is currently subdivided into three structural provinces according to their structural setting and regional dip direction [40], [41] (Fig. 1):

1-Northern Province: it represents the northern part of the GOS restricted by Galalahinge zone that extends on a line drawn from south Galala Plateau to the offshore of Asl Oil Field. The regional dip of strata is southwest; the main fault trends (the clysmic and the Aqaba) throw toward the northeast, and southeast, respectively [42].

2-Central Province: this province occupies the central part of the GOS. The regional dip is northeast. The main Clysmic and Aqaba trending throw towards the southeast and northwest, respectively.

3-Southern Province: this province is bounded from the north by the Morgan hinge zone bathing from the northern end of Esh El Mellaha to Ras Shukheir to the north of Muzhil. The regional dip of strata is towards southwest as the Northern Province and the main Clysmic and cross faults throw towards northeast and southeast, respectively [43].

2.4. Tectonic setting of the GOS

The extension of the GOS started at the early Oligocene; however, the separation between the African and Arabian plates did not begin until the early Miocene [10], [44] in general, two models have been proposed to describe how separation occurred [44]. The first model presumes that the GOS initiation resulted from the anticlockwise rotation of the Arabian plates relative to the African plate, with the center of rotation located at the center of the Mediterranean Sea. This model is widely used and agreed with the evident of magnetic anomalies across the central and southern of the Red Sea. The second model for the GOS initiation suggests that the initiation resulted from strike slip faulting and pulling apart tectonic across the axis of the rift. Although, many authors believe that this assumption requires more detailed studies to match the existing geometry, there is a slight match with the analysis of stratigraphic and outcrop structures By the Miocene end, the Arabian plate collided with the Eurasian plate, resulting in a change in the plate shape and development of the Dead Sea accompanied by suspension of the GOS rifting evolution [45].

2.5. Matulla Formation

Nezzaz Groups constituted of four formations namely (from top to bottom); Matulla, Wata, Abu Qada, and Raha, and made up of interbedded layers of shale, sandstone, siltstone, and limestone with a significant variation in mechanical properties (Fig. 2). This study focused on the Lower Senonian Matulla Formation. It is 140 m thick on average, and its lithology is composed of marls, limestones, and shales, with several sandstone units. The Matulla Formation unconformably overlies the Wata Formation. The upper part of the Matulla Formation is generally represented by sandy shales that grade into shales only toward the top.

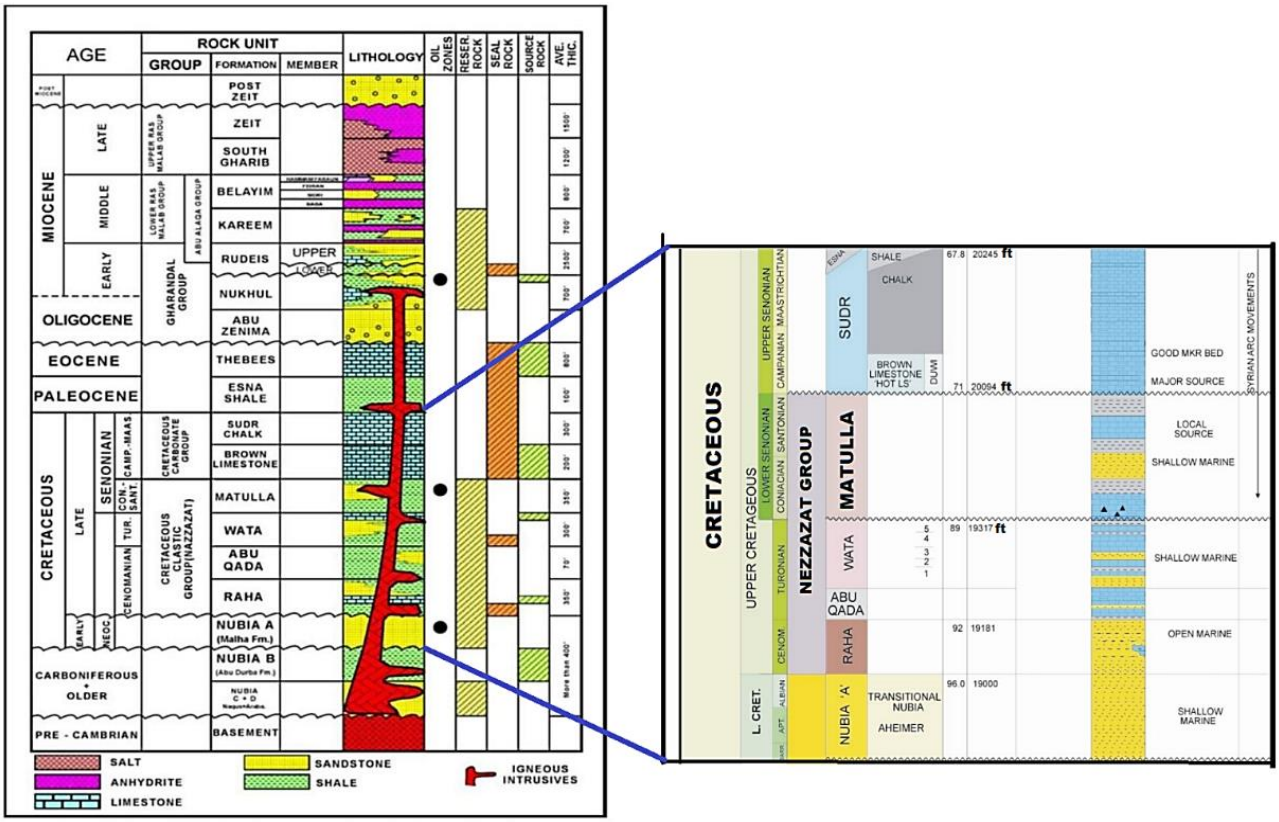

Figure 2. Generalized stratigraphic column of the Gulf of Suez [37]

A sharp break marks the onset of a different depositional environment of radioactive, dark brown, organic-rich limestones of the overlying Brown Limestone Member of the Sudr Formation [46].

The Coniacian-Santonian constitutes the wide range of sandstone reservoir in Pre-Miocene sequence. There are two main sub-units constituting Matulla Formation: the top is thinly interbedded sandstone and shale, while the bottom is clean sandstone with few inter-beds of shale and limestone [47]. This sandstone is the best reservoir in the Muzhil Field. This sandstone is white, medium to fine grained, sub-angular to angular, moderately sorted with calcareous cement, glauconitic and occasionally pyritic. The shale is gray, dark gray, light gray, soft, moderately hard, massive sub-flaky and highly calcareous. The limestone is dark brown, occasionally earthy white cryptocrystalline, hard to moderately hard, and argillaceous. The Matulla Formation was deposited in shallow marine conditions [48].

The Matulla Formation is separated between the overlying brown limestone formation and the underlying Wata Formation by two unconformity surfaces. All clastics of the Matulla Formation were deposited throughout the Coniacian-Santonian time span. Diverse planktonic foraminiferal contents, including Dicarinellaconcavata and Dasymetrica zones, revealing the Coniacian-Santonian age characterizes the Matulla Formation [9]. The Matulla Formation is composed of sandstone intercalated with shale, siltstones and carbonates. The deposition environment of this unit ranges from braided to meandering fluvial systems to shallow marine environments [47].

The Muzhil oil field is located in the central province of the GOS, with strata dip generally northeast, and is affected by many dikes which have recently been proven to have a high potential for hydrocarbon. The sandstone of the Matulla Formation, which is produced from the Nukhul and Matulla reservoirs, is an essential target for oil production in the Muzhil oil field.

Muzhil area is affected by regional Clysmic faults (Muzhil trend) with NW-SE direction which creates the main oil trap in the field on its up thrown. The termination of these oil fields is due to the intersection of the clays mic faults with the north oblique and/or northwest oblique faults. fault block started through the rifting phase during the Early Miocene, trap formation mainly occurred during the early rift rapid subsidence rate, affecting the pre-rift units (pre-Miocene) and early-rift units (Early Miocene) [49]. Faults formed during the Early Miocene which occurred first, followed by expulsion of the hydrocarbon, which creates the main oil in the field on its upthrown. The October field is located immediately to the west of the Muzhil block; it is a good analog to the subsurface play concept in the GOS as a general and in the SAZ block in particular.

3. Material and methods

3.1. Material

The available data are the complete set of open hole logs including caliper, total gamma ray, shallow and deep resistivity, density, neutron, sonic and photoelectric (PEF) from five wells in the Muzhil Field (Muzhil-1, Muzhil-2, Muzhil-4, Muzhil-7, and Muzhil-8) in addition to core analysis, pressure, and subsurface geological data supplied by the Egyptian General Petroleum Corporation (EGPC) and the SAZ. The well log analysis depended on equations, formulae, and pre-established charts and cross plots to study the Matulla Formation reservoirs by determining the petrophysical parameters using the computer software Techlog [50].

3.2. Vertical petrophysical evaluation methods

3.2.1. Lithological identification

The lithological identification of the Matulla Formation is of particular importance in the formation evaluation process because the physical and chemical properties of the rock that contains hydrocarbons and/or water affect the response of every tool used to measure the reservoir properties [51]. The most useful logs as indicators of lithological characteristics are gamma-ray, density, neutron, sonic, and photo-electric by using dia-porosity cross plots, tri plots as well as estimating the mineralogical components through least-squares models. The details regarding the use of cross plots combinations are discussed in [51]-[56].

3.2.1.1. Dia-porosity cross plots

Dia-porosity cross plots included the following:

1. Density (ρ_b) – Neutron (Φ_N) plots obtained using Schlumberger charts.

2. Matrix identification (MID) plots.

Clavier and Rust (1976) [57] proposed a cross plot that shows the separation of different matrix contents. The readings of the neutron, sonic, and density logs depend not only on the porosity, but also on the formation lithology and fluid content. When the appropriate matrix-lithology parameters (Δt_{ma}, ρ_{ma}, and Φ_{Nma}) are known, correct porosity values can be derived because accurate porosity determination becomes more difficult when the matrix lithology is unknown. A combination of the sonic, density, and neutron logs can establish more information about the formation and its contents than can be obtained from a single log.MID plots showing the relation between the apparent matrix densities, ($\rho_{b\,ma}$) and apparent matrix sonic travel time (Δt_{ma}) values, which are computed as follow [58], [59]:

For clean zones:

$$\rho_{ma} = \frac{\rho_b \cdot \log - \Phi_{\rho f}}{1 - \Phi}; \quad (1)$$

$$\Delta t_{ma} = \frac{\Delta t \cdot \log - \Phi \Delta t_f}{1 - \Phi}. \quad (2)$$

For shaly zones:

$$\rho_{ma} = \frac{\rho_b \cdot \log - \Phi_{\rho f} - V_{sh}\rho_{sh}}{1 - \Phi - V_{sh}}; \quad (3)$$

$$\Delta t_{ma} = \frac{\Delta t \cdot \log - \Phi \Delta t_f - V_{sh}\Delta t_{sh}}{1 - \Phi - V_{sh}}. \quad (4)$$

3. ρ_b-PEF plot in which bulk density (ρ_b) and the photoelectric effect PEF are cross plotted to provide an estimate of the mineral composition.

3.2.1.2. Tri plots

Tri plots include:

1. Plotting any two porosity log combinations in the *x*- and *y*-axes by taking GR as a third component (*z*-axis).

2. M-N cross plots that combine the data of the three porosity logs (ρ_b, Δt, and Φ_N) to provide lithology-dependent quantities, *M* and *N*, which are independent of the primary porosity [60]. Therefore, the cross plots of these two quantities make the lithological characteristics more apparent. *M* and *N* are defined as:

$$M = \frac{\Delta t_f - \Delta t_{ma}}{\rho_b - \rho_f} \cdot 0.01; \quad (5)$$

$$N = \frac{\Phi_{Nf} - \Phi_{Nma}}{\rho_b - \rho_f}, \quad (6)$$

where:

Δt_f – the transit time of fluid – 189;

Δt_{ma} – the transit time of the matrix;

Φ_{Nf} – 1.0;

Φ_{Nma} – the neutron porosity of the matrix;

ρ_b – the density log reading;

ρ_f – density of the fluid equals 1.03.

These results are usually confirmed using core analysis data and mud logs.

3.2.1.3. Mineralogical components using least-squares model

An appropriate estimate for the zone composition can be drawn from a least-squares model, in which the error is minimized between the log responses and their corresponding values predicted by the solution, Thus the matrix solution of the least-squares model becomes $V = (C^T \cdot C)^{-1} \cdot C^T \cdot L$, where each letter signifies an array of numbers or unknowns, rather than a single number of unknowns, as in conventional algebra. The "known" are *C* (vector of log readings), *L* (vector of log response), and the symbol C^T signifies the transpose of the *C* matrix, which simply means a matrix in which the rows and columns have been interchanged and the "unknown" is *V* (vector of the volume of minerals), as shown by [61]. On the other hand, if the log types (known data) are less than the unknowns (mineral volumes), the case is called underdetermined, and the matrix solution for the least-squares model becomes $V = C^T \cdot (C \cdot C^T)^{-1} \cdot L$.

Techlog software facilitated the complexities arising in the solution of the simultaneous equations. In this way, the correct values of the mineralogical constituents (quartz, calcite, dolomite, illite, and montmorillonite) were derived for the Matulla Formation in the studied wells (see the subsequent section of the lithosaturation cross plotting).

3.2.2. Shale evaluation

Shale evaluation is the next step in interpreting well logging. This includes three important processes: V_{sh} calculation, clay minerals identification, and shale distribution.

3.2.2.1. Shale volume calculation (V_{sh})

Reservoirs are usually differentiated into clean or shaly reservoirs based on the shale volume (V_{sh}) [62], [63] Increasing V_{sh} reduces both the reservoir quality and capacity. The most popular model used to calculate V_{sh} depends on the gamma ray (GR) log. This volume is the Shale Index (I_{sh}) as follows [62]:

$$I_{sh} = \frac{GR_{\log} - GR_{\min}}{GR_{\max} - GR_{\min}}, \quad (7)$$

where:

$GR_{\log}$ – gamma ray log reading for the zone of interest;

$GR_{\min}$ – minimum gamma-ray reading (clean sand or carbonate);

$GR_{\max}$ – maximum gamma-ray reading opposite to 100% shale.

It is customary to assume that $I_{sh} = V_{sh}$. However, this assumption tends to overstate the calculated V_{sh} [63]. Different empirical models have been developed to relate the shale index to V_{sh} according to the geological ages. The Matulla Formation is related to Cretaceous age; thus, two common models may be applied for older rocks in this study. After I_{sh} is considered, V_{sh} is calculated using any of the following equations suitable for consolidated and older rocks [64]:

Larionov (1969) [64]:

$$V_{sh} = 0.33\left(2^{2I_{sh}} - 1\right). \quad (8)$$

Clavier et. al. (1971) [57]:

$$V_{sh} = 1.7 - \sqrt{3.38 - \left(I_{sh} + 0.7\right)^2}. \quad (9)$$

It was observed that the two models provided very similar values. Clavier et.al. (1971) [57] model offers slightly lower values, and therefore, will be used here.

3.2.2.2. Shale types (clay mineralogy) identifications

The shale must be identified because of its significant effect on hydrocarbon reservoir evaluation. The clay minerals present in the reservoir can play the most important role, affecting both the reservoir capacity and production. The Archie water saturation equation assumes that the formation water is an electrically conductive material in formation. The presence of shale is another conductive material that complicates the definition or the concept of rock porosity. Thus, shaly formations may exhibit high Φ_t with a low Φ_e as a potential hydrocarbon reservoir. Clay minerals can be identified from spectral *GR* measurements (Thorium (Th), Potassium(K), and Uranium (U)) and Photoelectric log (PEF) using cross plots such as Thorium (Th) versus Potassium (K), PEF versus Potassium (K), and PEF versus Thorium over Potassium (Th/K) [65].

3.2.2.3. Shale distribution

The shaliness effect on log reading depends on the amount of shale and its physical properties. It may also depend on the way of the shale distribution in the formation. The shale can be distributed in the formation in three ways [65] (Fig. 3).

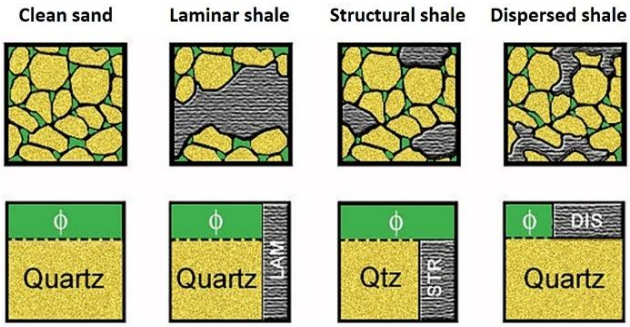

Figure 3. Distribution of shales in the reservoir [61], [63]

1. Laminar shale: shale can exist in the form of laminas between layers of sand. The laminar shale does not affect the Φ or the permeability of the sand streaks. However, when the amount of laminar shale is increased and the amount of porous medium correspondingly decreases, the overall average Φ_e is proportionally reduced.

2. Structural shale: shale can exist as grains or nodules in the formation matrix. This shale matrix is termed the structural shale. It is usually considered to have properties similar to those of the laminar shale and nearby the massive shale.

3. Dispersed shale: the shaly materials can be dispersed throughout the sand, partially if it fill the intergranular interstices. The dispersed shale may be in accumulations adhering to or coating the sand grains or it may partially fill the smaller pore channels. Dispersed shale in the pores markedly reduces the permeability of the formation.

These forms of shale can occur simultaneously in the same formation. Clay distribution was identified using the Techlog program and was confirmed by the GR versus DEN plot after [66], [67].

3.2.3. Determination of formation porosity (Φ)

Reservoir porosity is very important in calculating fluid saturation, which can be determined from density, neutron or sonic logs, and even their combination. The neutron-compensated, bulk density, and sonic logs were directly influenced by the matrix composition. Using two or three porosity log readings, it is possible to determine the porosity (Φ), and calculate the amount and type of each lithologic component: sandstone, limestone, and dolomite [58]. The total porosity (Φ_t) and effective porosity (Φ_e) were calculated for clean and shaly zones using the equations of [36] and [68].

3.2.3.1. Total porosity (Φ_t)

The total porosities derived using the density (Φ_D) and neutron (Φ_N) logs were calculated [36], [68]. The porosity derived from the bulk density log (Φ_D) is as follows:

$$\Phi_D = \frac{\rho_{ma} - \rho_b}{\rho_{ma} - \rho_f}, \quad (10)$$

where:

ρ_{ma} – the matrix density (sandstone = 2.65 g/cc);

ρ_b – the formation bulk density;

ρ_f – the fluid density (equal to 1.0 for fresh mud).

The porosity derived from the neutron logs (Φ_N) is expressed as follows:

$$\Phi_N = \Phi_{N\cdot\log} - \left(V_{sh} \cdot \Phi_{Nsh}\right), \quad (11)$$

where:

Φ_N – the corrected porosity for clean rock from shale;

$\Phi_{N\cdot log}$ – the reading of the neutron porosity from the log;

Φ_{Nsh} – the neutron porosity value for shale.

The total porosity can be obtained by combining the neutron and density porosity.

So, the total porosity equation in the absence of gas in the rock is as follows [62]:

$$\Phi_t = \frac{\Phi_D + \Phi_N}{2}. \quad (12)$$

3.2.3.2. Effective porosity (Φ_e)

This type of porosity depends largely on the degree of connection between the rock pores with each other forming channels, to facilitate the path of fluids (permeability) through the lithologic contents. The Φ_e was estimated using the following Equation 13 [51]:

$$\Phi_e = \Phi_t \cdot \left(1 - V_{sh}\right). \quad (13)$$

The average porosity values (ϕ) used in the qualitative description of reservoir rocks [52] are as follows: negligible ($\phi < 0.05$), poor ($0.05 < \phi < 0.1$), fair ($0.1 < \phi < 0.15$), good ($0.15 < \phi < 0.25$), very good ($0.25 < \phi < 0.30$), and excellent ($\phi > 0.30$).

3.2.4. Determination of formation water resistivity (R_w)

Precise knowledge of the formation water resistivity (R_w) is essential for correctly determining the S_w in the reservoir. Several methods can be used to determine formation water resistivity (R_w). Therefore, it is important to determine the value by matching and comparing the results with those obtained using various methods. In this study, R_w was determined using the formation water analysis method and accordingly, the R_w value of 0.13423 ohm-m at 22.3ºC was given for the Matulla formation (Table 1). The R_w was obtained using Equations 14 and 15 [69]:

$$R_{w75} = 0.0123 + \frac{3647.5}{NaCl^{0.955}}; \quad (14)$$

$$R_w = R_{w75} \cdot \frac{81.77}{f_t + 6.77}, \quad (15)$$

where:

R_w – formation water resistivity at the formation temperature;
R_{w75} – formation water resistivity at 75º;
F_t – is the formation temperature;
NaCl concentration in ppm (part per million).

Table 1. Laboratory water analyses are collected from DST or produced fluids in Matulla Formation at Muzhil-7 well

Total dissolved solids	53900 mg/l	pH	7.87 at 25ºC
Conductivity	$7.45 \cdot 10^{-2}$ mohs/cm at 22.3ºC	Density	1.03700 g/ml at 60 F
Resistivity R_w	0.13423 ohm-m at 22.3ºC	Specific gravity	1.03804
Salinity	51480 mg/l	Hardness	2408 mg/l

3.2.5. Fluids saturation estimation

3.2.5.1. Formation water saturation (S_w)

The determination of S_w is very important for determining the petrophysical parameters of the studied reservoir rocks. There are many equations for calculating S_w such as Archie, Dual Water, Indonesia, etc. The S_w for the examined zone was estimated by the Indonesia Equation which gives accurate results with shaly formation (Equation 16) [70][69]:

$$S_w = \left\{ \left[\left(\frac{V_{sh}^{2-V_{sh}}}{R_{sh}} \right)^{1/2} + \left(\frac{\varnothing_e^m}{a.R_w} \right) \right] R_t \right\}^{-1/n}, \quad (16)$$

where:

S_w – formation water saturation;
R_w – formation water resistivity (Ωm);
R_t – the true formation resistivity (Ωm);
a – the tortuosity factor;
m – the cementation factor;
n – saturation exponent.

The equation requires the resistivity log (R_t), $\Phi_e \cdot \log$, $V_{sh,}$ and formation water resistivity R_w. The inputs for the S_w model parameters (R_w, a, m, and n) were based on information from the fluid samples, logs, and special core analysis measurements (Table 2).

Table 2. The applied parameters for the applied saturation model (the Indonesia equation)

Parameter	Value	Source
R_w	0.13423 ohm-m at 22.3ºC	Laboratory water analysis
a	1	From the special and routine core analysis of the wells Muzil-4, Muzhil-7 and Muzhil-8
m	1.81	
n	1.83	

After converting a water analysis to an equivalent NaCl concentration, several water samples were analyzed at a depth of 11100 ft within the Matulla formation in the Muzhil-7 well, and the R_w was found to be 0.055 Ω.m at 22.3ºC (surface temperature) (Table 1).

The formation water resistivity can be corrected from its value at laboratory temperature to the formation temperature either by using a chart found in most logging manuals or by Arp's empirical formula [71].

3.2.5.2. Bulk volume of water (*BVW*)

The bulk volume of water was estimated using the following equation of [72]:

$$BVW = \Phi_e \cdot S_w, \quad (17)$$

where:

BVW – the bulk volume of water;
Φ_e – the effective porosity;
S_w – water saturation.

3.2.5.3. Hydrocarbon saturation (S_h)

The fraction of pore space containing water is termed water saturation (S_w). The remaining fraction, containing oil or gas, is termed hydrocarbon saturation (S_h). The total hydrocarbon saturation (S_h) was calculated using the following Formula (18):

$$S_h = 1 - S_w. \quad (18)$$

S_h is usually differentiated into its residual (S_{hr}) and movable (S_{hm}) fractions, which can be calculated from water saturations in the uninvaded and flushed zones (S_w and S_{xo}), as follows:

$$S_{hr} = 1 - S_{xo}; \quad (19)$$

$$S_{hm} = S_h - S_{hr}, \quad (20)$$

where:

S_{hr} – the residual hydrocarbon saturation in the invaded zone;
S_{xo} – S_w in the invaded zone;
S_w – the water saturation in the uninvaded zone;
S_{hm} – the movable hydrocarbon saturation.

Net reservoir, Net Pay and Reservoir Cutoffs

"Net reservoir" is defined as the thickness of rocks having high porosity and low shale content. "Net Pay" is defined as the thickness of rock that contributes to economically viable production with today's technology, prices, and costs. Net pay is obviously a moving target, because technology, prices, and costs vary almost daily. We determine net pay by applying appropriate cutoffs to reservoir properties, so that unproductive or uneconomic layers are not counted. This can be done with both log and core data, and it is normal to apply cutoffs to each calculated result to eliminate poor-quality or unproductive zones. Cutoffs are usually applied to V_{sh}, ϕ and S_w. The following cutoff parameters were used in this study: $V_{sh} < 0.5$, $\Phi_e \leq 0.10$ and $S_w < 0.5$.

3.2.5.4. Fluid type determination

The Modular Formation Dynamics Tester Tool (MDT)

The MDT tool provides the capability to conduct fluid sampling, controlled local production, standard transient and vertical interference tests. Such interval tests usually comprise a drawdown and buildup-typically, the tool is stationed in the borehole, and two packers are set to hydraulically isolate a section of the formation. Observation probes or multiple probes mounted above the packers provide the capability for vertical interference testing within the near-wellbore formation.

The methodology used to analyze the MDT transient data is similar to that conventional pressure transient tests. However, specialized mathematical models are used to match the pressure and flow rate measurements. Conventionally, analytical models have been used to analyze these tests. Although computations of analytical models are fast, they may be too simplistic or inadequate for many test configurations. On the other hand, numerical models are more realistic and flexible. However, their use is complex. Therefore, we propose an integrated approach in our interpretation methodology.

Gradient based techniques have been used in reservoir simulation for history matching of the pressure and production performance of reservoirs for some time. In current study we focused on their application to MDT interval pressure transient tests in combination with numerical well testing methods [73], [74].

Integrated MDT analysis

The objective was to present the analysis that was performed for all the pressure data points recorded in Muzhil field reservoirs (Matulla Formation) [75]. In each well to determine the fluid type and fluid contacts. Then to integrate and investigate the communication between the wells "if any" considering, all the available data with the study team to confirm these results. The pressure point was plotted against true vertical depth and based on the pressure gradient on the plot.

3.3. Horizontal petrophysical evaluation methods

3.3.1. Isoparametric maps

Lateral variation of petrophysical characteristics could be studied from constructed isoparametric maps. The study of these petrophysical parameters maps is very important in judging their lateral variation and the factors that control them, which may be either stratigraphic, structural, or both.

3.3.2. Hydrocarbon volume estimation

In this study the hydrocarbon volumes for the Matulla reservoir were estimated by Equation (21) and (22) that proposed for hydrocarbon calculations [76]. Hydrocarbon volumes are computed using parameters inputted into the static reservoir model and accuracy of the volumetric depends on the integrity of porosity (Φ), saturation, net thickness, areal extent, and formation volume factor values.

Equation (21) can be applied to calculate Stock Tank Oil Initially in Place (STOIIP):

$$N = \frac{7758Ah\Phi \cdot (1 - S_{wi})}{B_{oi}} \text{ (STB).} \quad (21)$$

Equation (22) can be applied to calculate free gas (GIIP) in a gas reservoir as given below:

$$G = \frac{43560Ah\Phi \cdot (1 - S_{wi})}{B_g} \text{ (MM SCF),} \quad (22)$$

where:

N – STOIIP [barrels];

G – GIIP [MM SCF];

A – area [acres];

h – net pay thickness [feet];

7758 – conversion factor (acre-ft·7758 = barrels);

Φ – porosity of this net reservoir rock (decimal);

S_w – irreducible water saturation – water-filled portion of this porosity (decimal);

B_{oi} – formation volume factor for oil (decimal), expresses the change in oil volume between reservoir and standard conditions at the surface (reservoir barrels/stock tank barrels);

S_g – gas saturation ($1 - S_{wi}$) is traditionally omitted from equation (22).

Oil formation volume factor (B_{oi}) can be defined as the ratio of volume at reservoir condition to volume at the surface condition (at 60ºF and 14.7 psi). It usually varies from 1.0 to 1.7. A formation volume factor of 1.4 is characteristic of high-shrinkage oil and 1.2 of low-shrinkage oil, in the case of gas calculation the (B_{oi}) is replaced by (B_g).

4. Results and discussions

4.1. Lithological identification of Matulla Formation

4.1.1. Neutron-density cross plots

Figure 4 represents the relation between ρb and Φ_N with taking the *GR* as a third component. The first glance reveals that the majority of the presented points in these plots lie between the limestone, dolomite, and the sand line with high and medium *GR* intensity for the Matulla Formation in Muzhil-1, -2, -4 and -7 wells, indicating the presence of shale.

Neutron-density cross plot for of Matulla Formation in Muzhil-1 well (Fig. 4a) shows that the major lithology is tight limestone with some stricks of shale, and sandstone with some effect of the presence of shale shifted the points Whereas the Neutron-density cross plot (Fig. 4b) in Muzhil-2 well, shows that the major lithology is sandstone with an amount of limestone and there is a trend of points toward shale. In Muzhil-4 and Muzhil-7 wells the neutron-density cross plot (Fig. 4), show that the major lithology is calcareous sandstone, and there is a trend of points toward shale. The Φ values range from 10 to 25% in all the studied wells (Fig. 4).

4.1.2. M-N cross plots

Tri-porosity (M-N) cross plots are used to generally determine the lithology of the Matulla Formation in the studied area, which showed that the main lithology type is sandstone with cementation of limestone intercalated with shale (Fig. 5).

4.1.3. MID cross plots

The matrix identification plots (MID) for the Matulla Formation in the Muzhil-1and Muzhil-7 wells are presented in Figure 6 showing that the majority of the data points are concentrated around the calcite points, illustrating and confirming that the major lithology is sandstone with limestone, and the remaining points suggest the existence of shale and heavy minerals.

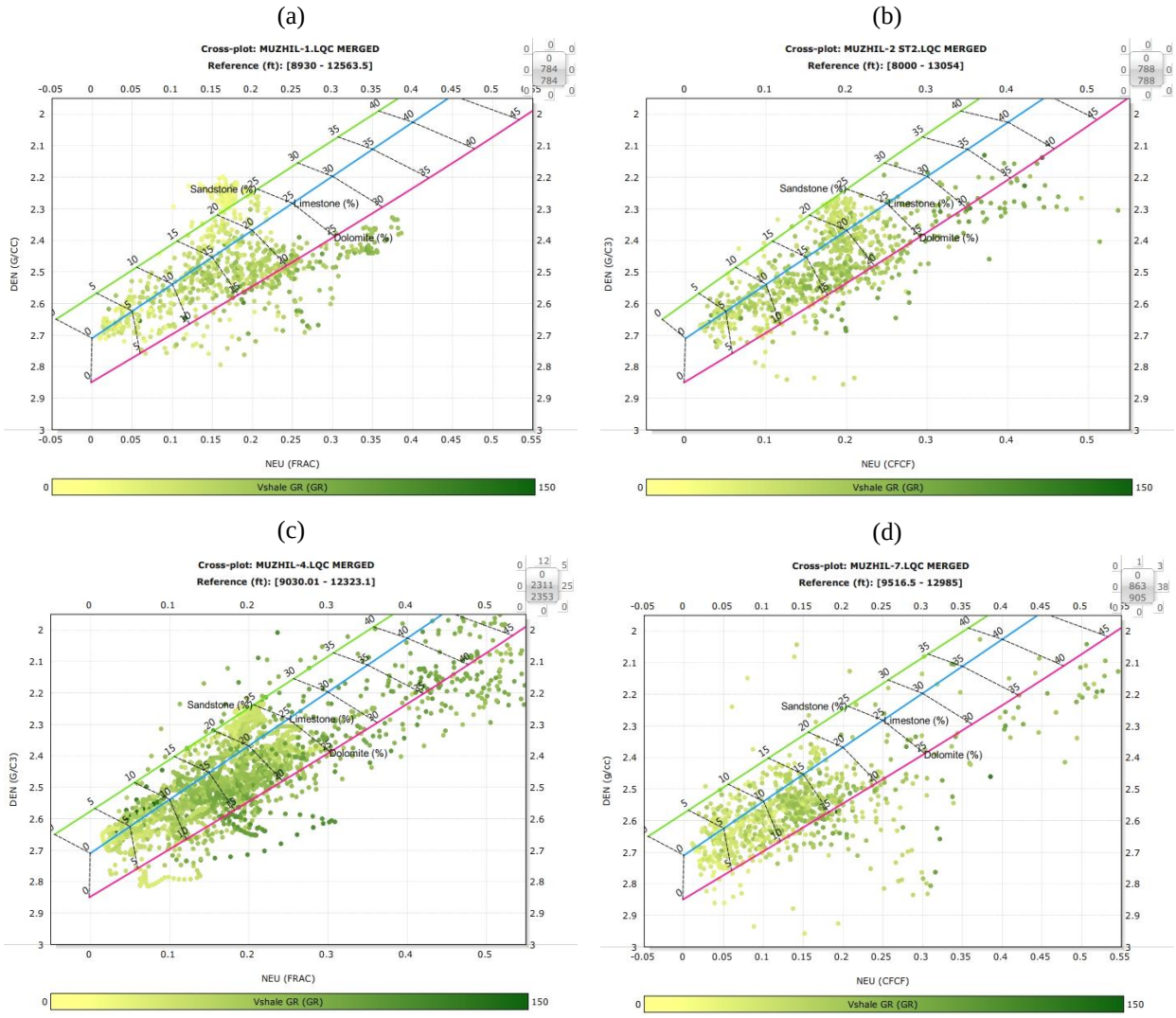

Figure 4. Neutron-Density cross plot for Matulla Formation: (a) Muzhil-1 well; (b) Muzhil-2; (c) Muzhil-4 well; (d) Muzhil-7 well

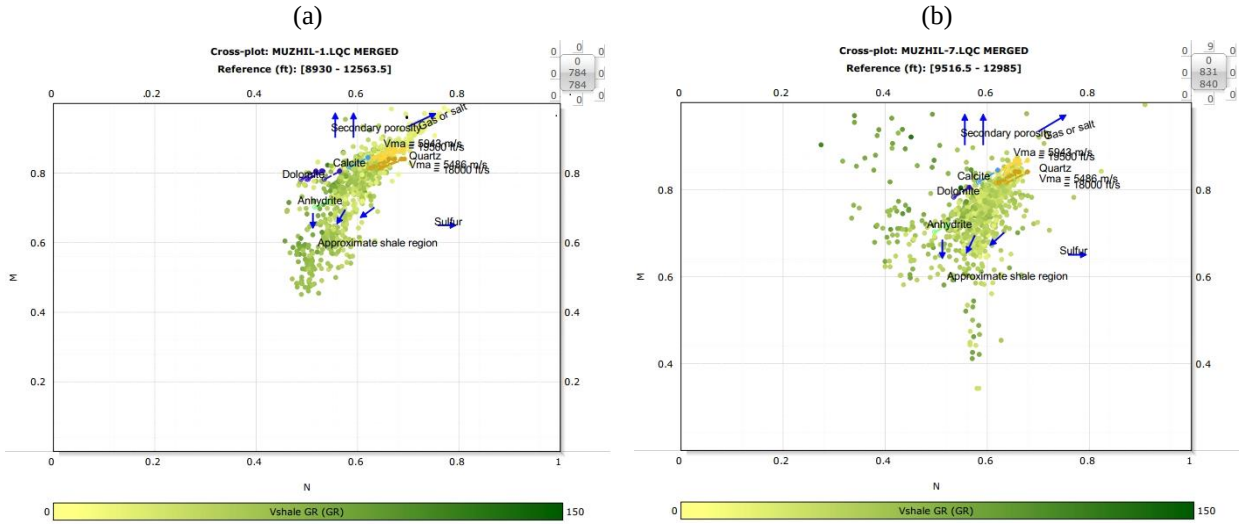

Figure 5. M-N cross plot for Matulla Formation: (a) Muzhil-1 well; (b) Muzhil-7 well

In MID Cross plots (Fig. 6), a few points are found around the dolomite point. This is with a remarkable lack of secondary porosity and gas effects.

The most striking feature observed is that the quartz area is completely barren.

4.1.4 ρ_b-PEF cross plots

The ρ_b-PEF cross plot are plotted for the Matulla formation in Muzhil-1 and Muzhil-7 wells (Figs. 7, 8), reveling that the Matulla formation in all studied wells is mainly composed of dolomitic sandstone, shale, and dolomite.

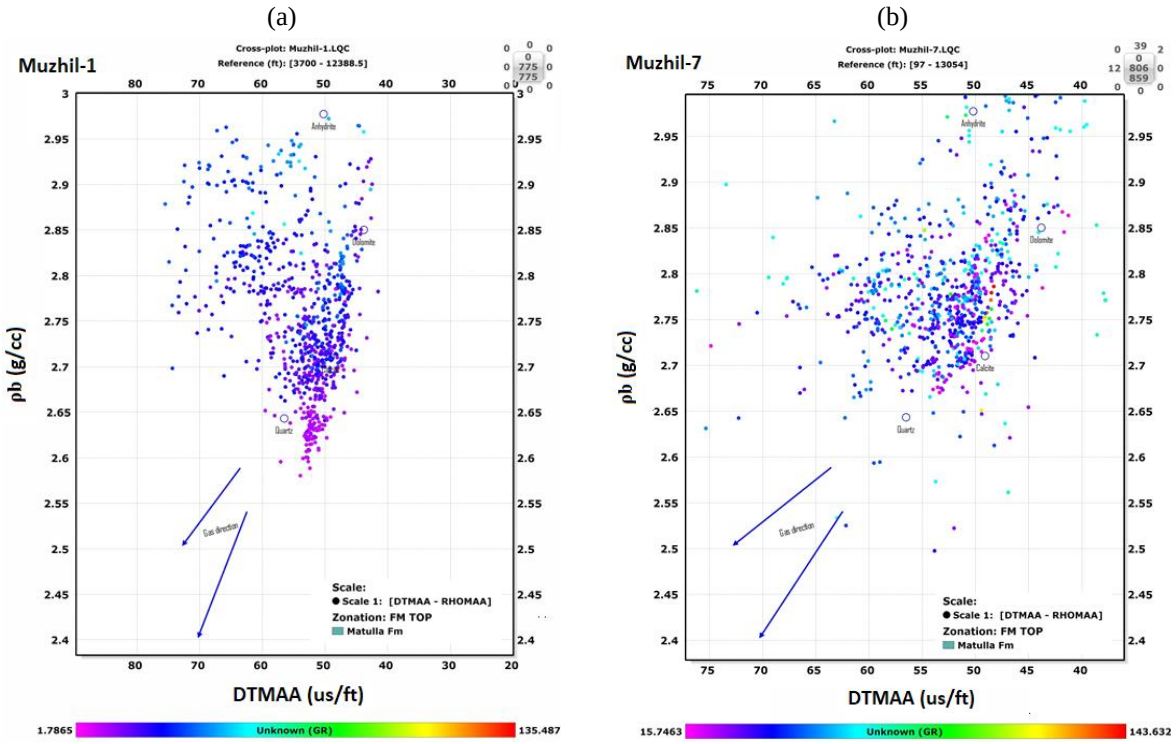

Figure 6. MID Cross plots of the Matulla Formation: (a) Muzhil-1 well; (b) Muzhil-7 well

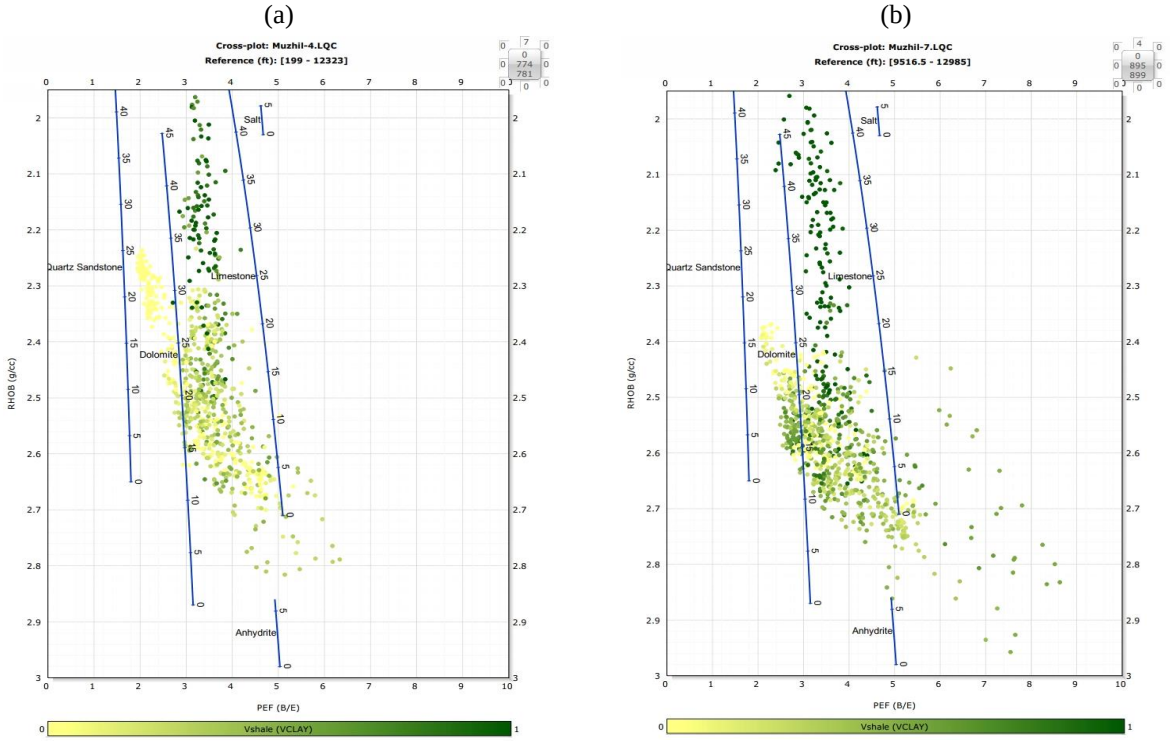

Figure 7. RHOB-PEF cross plot for Matulla Formation: (a) Muzhil-1 well; (b) Muzhil-7 well

Where the dolomite and the dolomitic sand show low clay content (yellow points) and the shale (dark green points) reflect the high clay content.

4.2. Shale evaluation of Matulla Formation

4.2.1. Shale volume (V_{sh})

Precise estimation of the V_{sh} is essential in the petrophysical evaluation of clastic reservoir rocks since it is vital in discrimination between non-reservoir and reservoir rocks. *GR* logs were used to calculate the V_{sh} in Matulla Formation for the five wells scattered in the Muzhil Oil Field (Table 3).

4.2.2. Shale types (clay mineralogy)

To evaluate the type of shale, whether effective (montmorillonite and illite) or non-effective (kaolinite and chlorite), a number of cross plots (Th-K, PEF-K, and PEF-Th/K ratio) (Figs. 9-11) are established in Muzhil-2, and Muzhil-8 wells (for example), to identify clay minerals in Matulla Formation, reflecting a mixed nature of minerals such as montmorillonite, mixed layer clays, chlorite, and kaolinite.

Therefore, the major type that existed is montmorillonite, which has a high effect on the Φ of the reservoir.

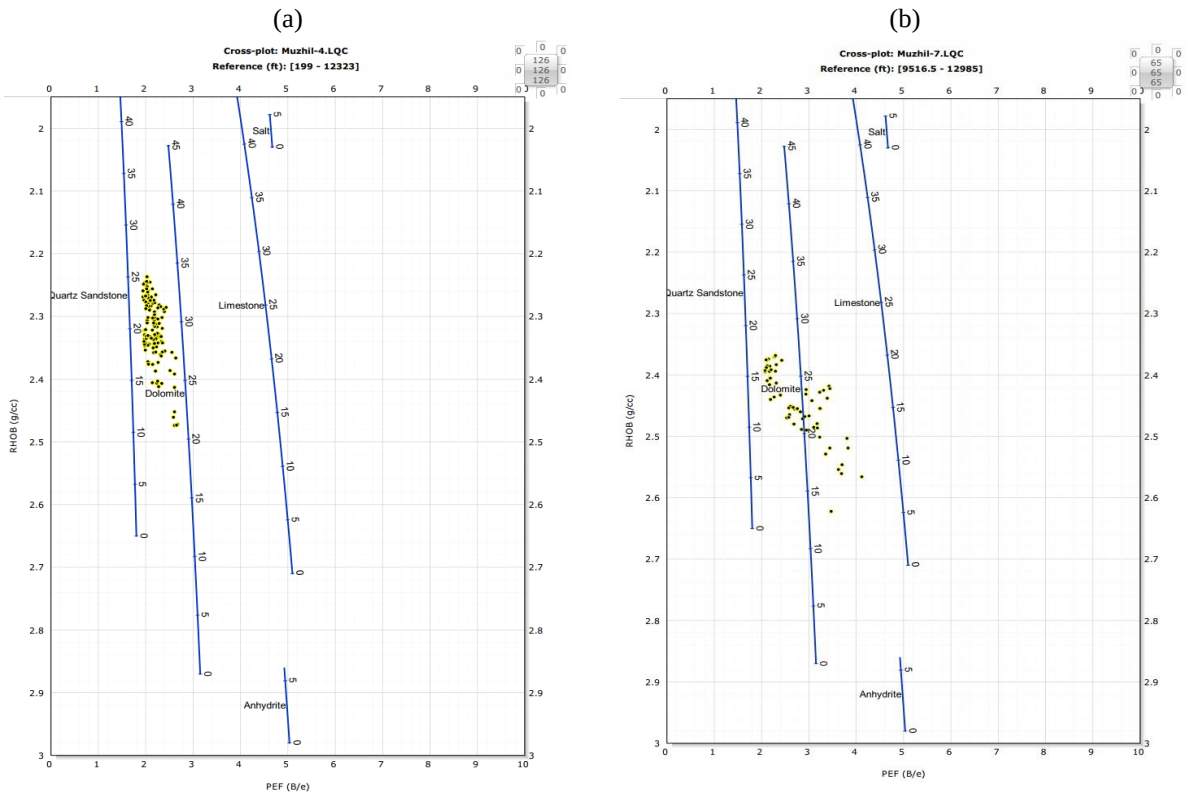

Figure 8. RHOB-PEF cross plot for Matulla Formation: (a) Muzhil-1 well; (b) Muzhil-7 well

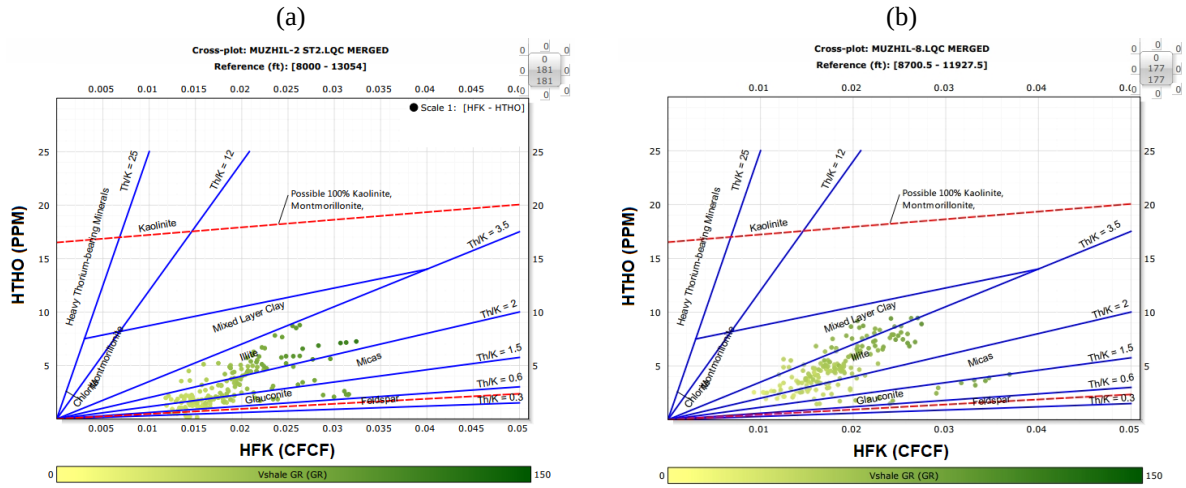

Figure 9. Cross plot analysis for clay minerals identification, Thorium vs. Potassium for Matulla Sandstone: (a) Muzhil-2 well; (b) Muzhil-8 well

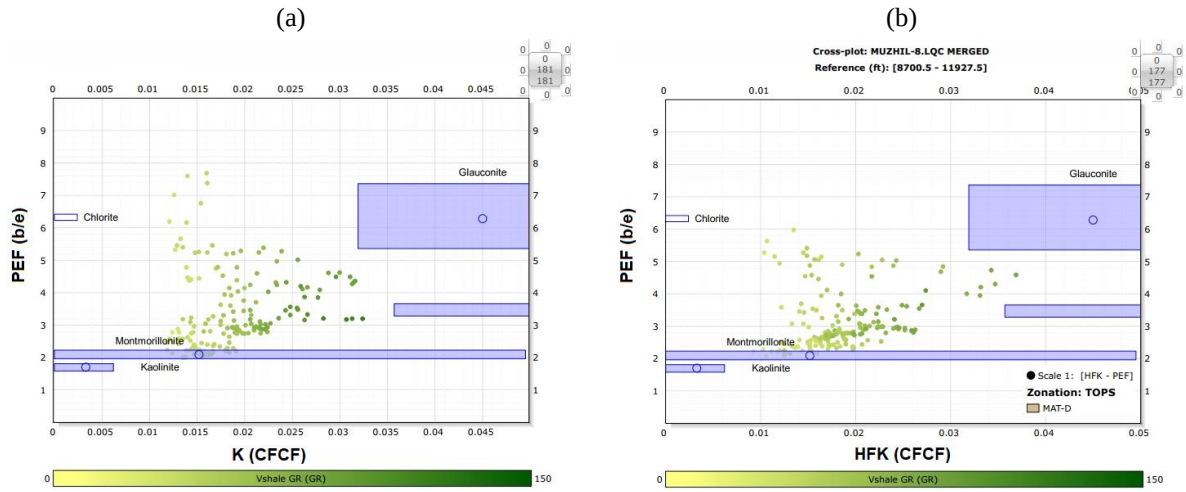

Figure 10. Cross plot analysis for clay minerals identification Potassium vs. PEF, for of Matulla Sandstone: (a) Muzhil-2 well; (b) Muzhil-8 well

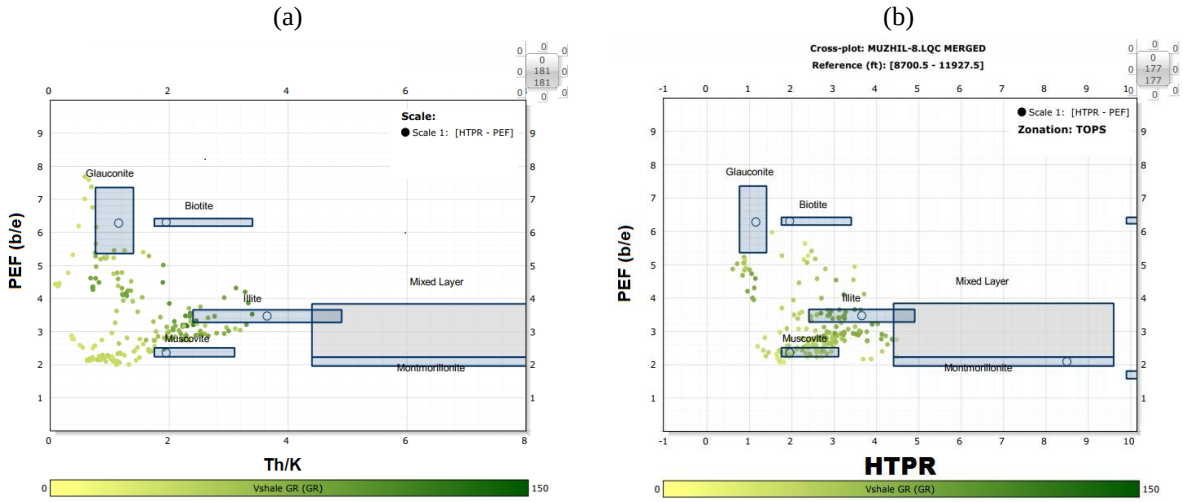

Figure 11. Cross plot analysis for clay minerals identification, Thorium to Potassium ratio log vs. PEF of Matulla Sandstone: (a) Muzhil-2 well; (b) Muzhil-8 well

Table 3. Summary of the average petrophysical parameters of Matulla Formation in the studied wells

Well		Muzhil-1	Muzhil-2	Muzhil-4	Muzhil-7	Muzhil-8
Top (ft)		11107	11629	11280	12144	11135
Bottom (ft)		11499	12023	11672	12596	11539
Gross Thickness (ft)		392	394	392	452	404
Net reseroir thickness (ft)		86	62	68	13	106
Net pay thickness (ft)		83	60	0.0	0.0	0.0
N/*G*, v/v		0.21	0.15	0.00	0.00	0.00
BVW, v/v		0.06	0.03	0.15	0.21	0.18
Weighted Average	Φ_t, v/v	0.18	0.18	0.18	0.23	0.20
	Φ_e, v/v	0.15	0.15	0.16	0.19	0.18
	V_{sh}, v/v	0.21	0.26	0.37	0.35	0.40
	S_w, v/v	0.38	0.20	0.82	0.92	0.7
	S_{hc}, v/v	0.62	0.80	0.18	0.09	0.00
	S_{hmov}, v/v	0.47	0.65	0.03	0.07	0.00
	S_{hirr}, v/v	0.15	0.15	0.15	0.02	0.00
	K, md	44.62	94	232.21	0.17	281.07
Variation Range	Φ_t, v/v	0-0.25	0-0.30	0-0.47	0-0.47	0-0.28
	Φ_e, v/v	0-0.23	0-0.28	0-0.47	0-0.35	0-0.27
	V_{sh}, v/v	0-1	0.03-1	0.17-1	0.08-1	0.09-0.98
	S_w, v/v	0-1	0-1	0-1.0	0.32-1	0.3-1
	S_{hc}, v/v	0-1	0-1	0-1	0- 0.68	0-0.7
	S_{hmov}, v/v	0.05-0.23	0-0.19	0- 0.20	0-0.0	0-0.0
	S_{hirr}, v/v	0-0.23	0-0.25	0-0.26	0-0.0	0-0.0
	K, md	0-639	0-184.6	0-3637	0-0.75	0-606

In addition, the photoelectric effect (*PEF*) has a wide range of values, reflecting a mixed nature of minerals. The radioactivity level of uranium is high especially in the lowest part of this well, revealing shales and carbonates of organic affinity (source rocks).

4.2.3. Shale distribution and impact on reservoir quality

According to the model of Thomas and Steiber [67], the cross plots of *GR*-ρ_b have been plotted using the Techlog program and used as a tool for clay distribution identification (Fig. 12a, b). For example, *GR*-ρ_b plots of Muzhil-1 well show that clays are mostly distributed within the sandstone of Matulla Formation in laminated and dispersed forms with slight effect (Fig. 12a), where as the *GR*-ρ_b cross plot of Muzhil-2 shows variations from clean to laminated and dispersed clay distribution in (Fig. 12b).

4.3. Petrophysical parameters and hydrocarbon potentiality of the Matulla Formation

The average and limits of all petrophysical parameters (shale volume, total and effective porosities, fluid saturation (water and hydrocarbons), permeability, gross thickness, net reservoir thickness, net pay, *N*/*G*, and *BVW*) of the Matulla Formation zone in the five wells (Muzhil-1, Muzhil-2, Muzhil-4, Muzhil-7, and Muzhil-8) are listed with the estimated gross thickness, net thickness, *N*/*G* and *BVW* values in Table 3.

On the other hand, all petrophysical characteristics and the corresponding hydrocarbon potentiality of the Matulla Formation deduced from the well-log analysis are presented and studied through two main stages. The first stage is the vertical distribution of petrophysical parameters, which has been performed in the course of the litho-saturation cross plots constructed for Matulla Formation in the 5 studied wells in Muzhil Field using the Techlog software (Fig. 13a-e).

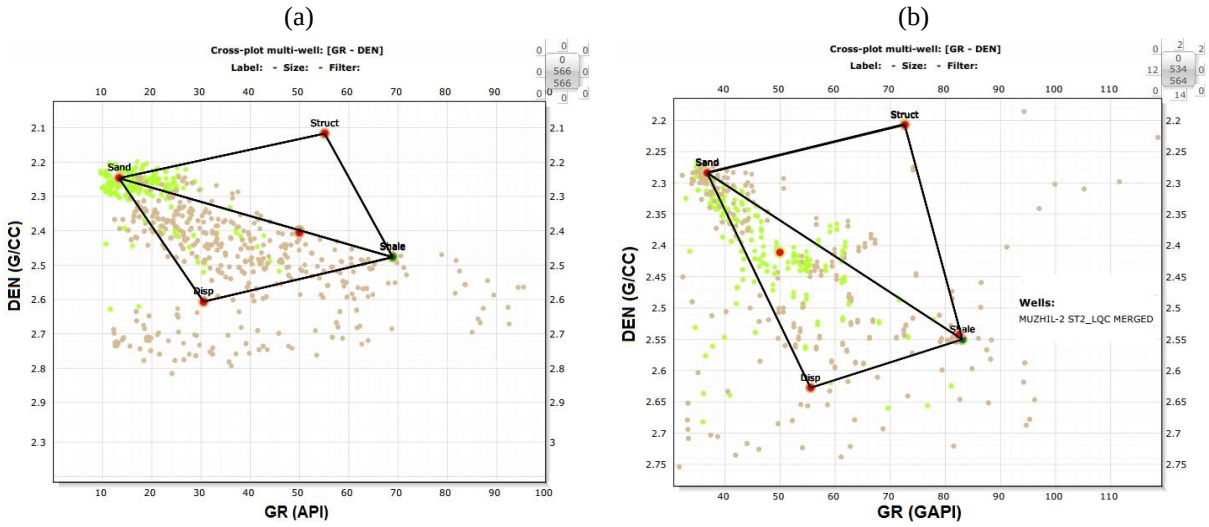

Figure 12. Shale distribution identification through Thomas and Steiber cross plot of Matulla Formation in Muzhil-1 (a) and Muzhi-2 (b) wells

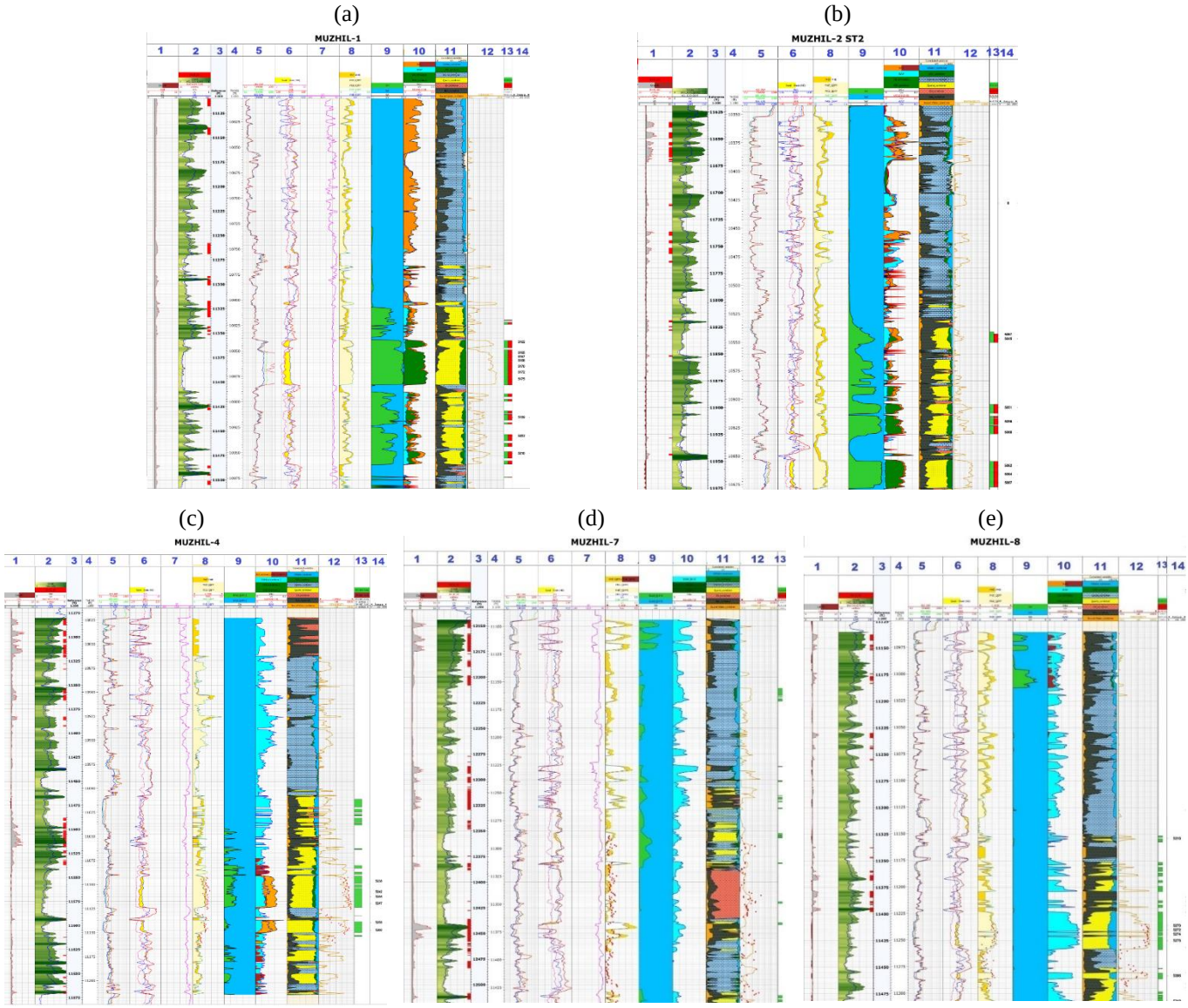

Figure 13. Litho-saturation cross plot showing the vertical distribution of the different petrophysical parameters in the sediments of Matulla Formation in: (a) Muzhil-1 well; (b) Muzhil-2 well; (c) Muzhil-4 well; (d) Muzhil-7 well; (e) Muzhil-8 well

The second stage is the lateral variation of petrophysical parameters in the course of the constructed isoparametric contour maps, including shale content (V_{sh}), effective porosity (Φ_e, %), net pay thicknesses, hydrocarbon saturation (S_h, %), as well as the hydrocarbon volume, to complete the vision of hydrocarbon potentialities of Matulla reservoir in the studied area (Fig. 18a-f).

4.3.1. Vertical distribution of petrophysical characteristics

The litho-saturation cross plots are constructed for the Matulla Formation in all studied wells in Muzhil Field using the Techlog software (Fig. 13a-e). In each cross plot, the calliper (CAL) log is displayed in Track 1. GR, shale content (Vsh), and bad hole flags are displayed in Track 2. Tracks 3 and 4 exhibit the measured reference depth and true vertical depth (TVDSS). Track 5 shows deep, medium, and shallow resistivity logs (LLD, LLM, and LLS). Track 6 displays density (DEN), neutron (CNL), and photoelectric (PEF) logs. Track 7 presents the sonic (ΔT) log. Track 8 demonstrates the estimated true and effective porosity (Φ_t and Φ_e) predicted from logs in all wells that are close to those obtained from core data (red dots, only in Muzhil-4, Muzhil-7, and Muzhil-8wells). Track 9 compares the log-derived water and hydrocarbon saturations (S_w and S_h). Track 10 presents the bulk volume of water (*BVW*), movable hydrocarbon saturations (S_{hmov}), and residual hydrocarbon saturations (S_{hirr}). Track 11 displays the results of mineralogical and fluid components in volume percentage (decimal) estimated by using the least-squares model with core data. Track 12 presents the permeability results predicted from logs in all wells close to that obtained from core data (red dots, only in Muzhil-4, Muzhil-7, and Muzhil-8 wells). Track 13 demonstrates the flags of the net reservoir and net pay zones. Track 14 exhibits the measured pressure data (only in Muzhil-1, Muzhil-2, Muzhil-4, and Muzhil-8wells).

Litho-saturation cross plot of Muzhil-1 well (Fig. 13a and Table 3) represents the different petrophysical parameters in the Matulla Formation which extends from 11107 to 11499 ft with a thickness of 387 ft and a reservoir thickness of 86 ft the Matulla Formation in this well has 83 ft Net pay, Φ_e of 15% and S_w of 38%. Lithologically it is composed of mixed clastic rocks (sand and shale) with some limestone. The Matulla formation has an average V_{sh} of 21%. The Φ_e mean value of 15%, S_w of 38%, and S_h of 62% (the average value of S_{hmov} is 47%, and S_{hirr} is 15%). The Matulla Formation in Muzhil-1 has a good reservoir possibility.

Fig. 13b and Table 3 represent the vertical distribution of the different petrophysical parameters in the sediments of Matulla Formation in Muzhil-2 well. The rock units in this interval are composed of clastic (sandstone and shale) with feldspar, in addition to little calcareous cement and shale content. Within Matulla Formation, feldspar has a little different distribution which decreases in the lower part. The average of V_{sh} is 26%, Φ_e is 15%, S_w is 20%, S_h is 80% and S_{hmov} is 65% indicating that the Matulla Formation in Muzhil-2 has good reservoir possibility.

In Muzhil-4 well, the studied Matulla Formation extends from 11280 to 11672 ft, with a gross thickness of 392 ft and a reservoir thickness of 68 ft (Fig. 13c and Table 3). It consists mainly of carbonate with sandstone and shale. The V_{sh} is 37% and this is accompanied by decreasing the volumes of sandstone, and carbonate. Whereas the average Φ_e is 16% and it ranges from 0 to 47% S_w range is 0-100% with an average reaches 82%, whereas the S_h increases to18%. S_{hmov} is 3%. Matulla formation in Muzhil-4 well has not fair conditions for reservoir possibility (Fig. 13c and Table 3).

The processed interval of Matulla Formation sediments in Muzhil-7 well extends from 12144 to 12596 ft (Fig. 13d and Table 3) and consists of mixed lithology from sandstone, siltstone, shale, and some streaks of limestone. The V_{sh} is 35%, Φe varies from 0 to 47% , with mean value of 19%. S_w increases in Matulla formation (32 to 100%) with weight average is 92%. The sandstone is very low in Matulla Formation in this well. Whereas S_h is absent. Matulla Formation in Muzhil-7 well produces water only.

Litho-saturation cross plot of Muzhil-8 Well extends from 11135 to 11539 ft, with a gross thickness 404 ft, and a reservoir thickness of 106 ft. Litho-saturation cross plot illustrates lithology mixed from sandstone, siltstone, shale, and limestone (Fig. 13e and Table 3). The value of V_{sh} from 9 to 98%, with an average 40 and this is accompanied by decreasing volumes of sandstone and carbonate The Φ_e varies from 0 to 27%, with a weight average of 18%. S_w ranges from 30 to 100%, with an average of 70%, whereas S_h is absent in Matulla formation. Accordingly, Matulla Formation in Muzhil-7 well produces water only.

Generally, the total Matulla Formation in the 5 wells has relatively low V_{sh} values with an average of 31.8%, a maximum value of 40%, and minimum value of 21%. The high *GR* readings in the main Matulla reservoir are related to the feldspar content. Good Φ_e values of the Matulla Formation are observed with a maximum value of 19% and a minimum value of 15% and average value of 16.6%. The S_w reflects an average value of 66%, with a maximum value of 100% in Muzhil-8 well and a minimum value of 20% in Muzhil-2 well. The hydrocarbon saturation (S_h) shows high values in Muzhil-1 and Muzhil-2 wells. The average S_h in the Matulla reservoir is 31%, with a minimum value of 0% in Muzhil-8 and a maximum value of 62% in Muzhil-1 well. The estima-ted permeability (*K*) in Matulla reservoir shows an average value of 281 mD, with a maximum of 281 mD in Muzhil-8 well and a minimum one of 0.3 mD in Muzhil-7 well (Table 3). Primarily, the petrophysical evaluation indicates the occurrence of a good sand reservoir of low resistivity logs and relatively different petrophysical characteristics (Table3). Oil bearing zones in Muzhil-1 and Muzhil-2 and 100% water zone in Muzhil-8 well reservoirs could be detected.

The Φ_t of Matulla Formation sediments ranges from 0 to 47% with average values of 18, 17.5, 19, 23, and 20% for Muzhil-1, Muzhil-2, Muzhil-4, Muzhil-7 and Muzhil-8, respectively, while the Φ_e ranges from 0 to 47% with an average Φ_e of 15, 15, 16, 19, and 18%, respectively. The vertical distribution of Φ shows the upward increase in the values, and the highest values often coincide with minimal content of clays (Fig. 13a-e). The Φ type is commonly determined by plotting neutron-density Φ versus sonic Φ. The plot reveals the abundance of inter-granular Φ particularly in the quartzose sandstones and secondary Φ in the calcareous sands. V_{sh} ranges from 0 to 100% with the average values of 21, 26, 37, 35, and 40% for Muzhil-1, Muzhil-2, Muzhil-4, Muzhil-7, and Muzhil-8, respectively. Shale is distributed mainly in a laminated and dispersed form, and which reduces the pore space. Matulla Formation exhibits higher S_w values compared to hydrocarbon saturation with average values of 38, 20, 82, 92, and 100% for Muzhil-1, Muzhil-2, Muzhil-4, Muzhil-7 and Muzhil-8, respectively. The highest values of S_w are often associated with the sandstones containing clays, while the lower values mainly correlate with shale. Cutoffs of 10, 50, and 50% for Φ, S_w, and V_{sh} are applied to differentiate between pay and non-pay zone intervals (Table 3).

4.3.2. Verification of estimated results

In the Matulla formation of Muzhil Field, the sandstone represents the only reservoir where carbonates have no opportunity to produce hydrocarbon because of the reservoir characters represent very low porosity and permeability. Porosity can be restored and enhanced at depth.

Tracks 8 in Figure 13c-e demonstrate the estimated porosity estimated from well logs in wells Muzhil-4, Muzhil-7, and Muzhil-8 that are close to those obtained from core data (red dots). Also, Tracks 12 in Figures 14, 15, and 16 present the permeability results predicted from well logs in wells Muzhil-4, Muzhil-7 and Muzhil-8 close to that obtained from core data. The correlations between the measured porosity and permeability from core samples with those calculated from well log interpretation, respectively, show a fair to good degree of agreement, which assures those calculated in the other wells where no core samples are available.

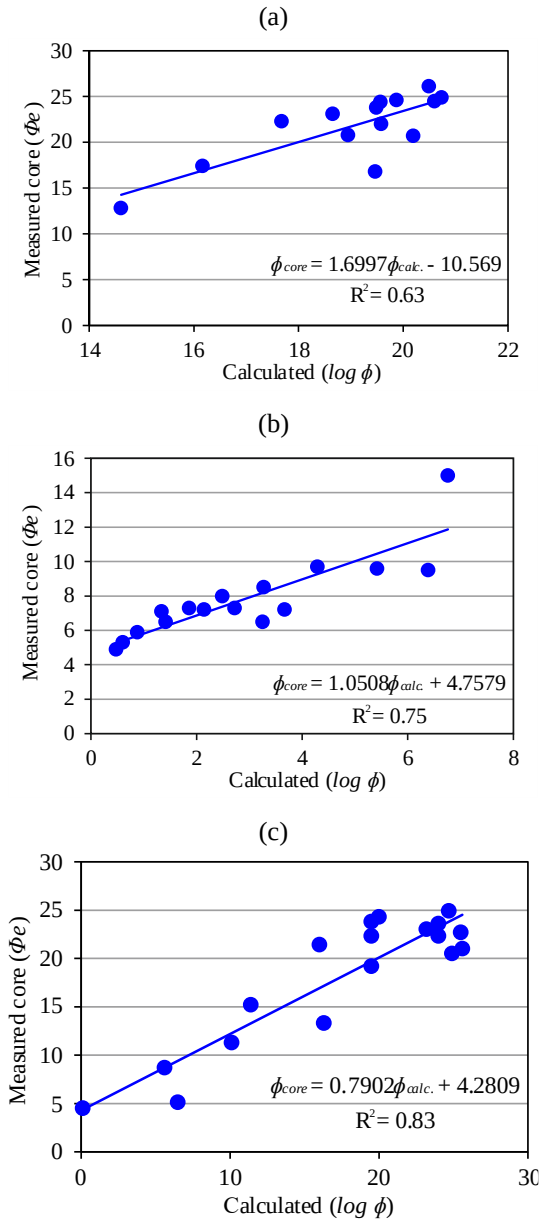

Figure 14. Measured core porosity and calculated log porosity (Φ_e) validation for Matulla: (a) Muzhil-4 well (11541-11579); (b) Muzhil-7 well (12390-12434); (c) Muzhil-8 well (11396-11451)

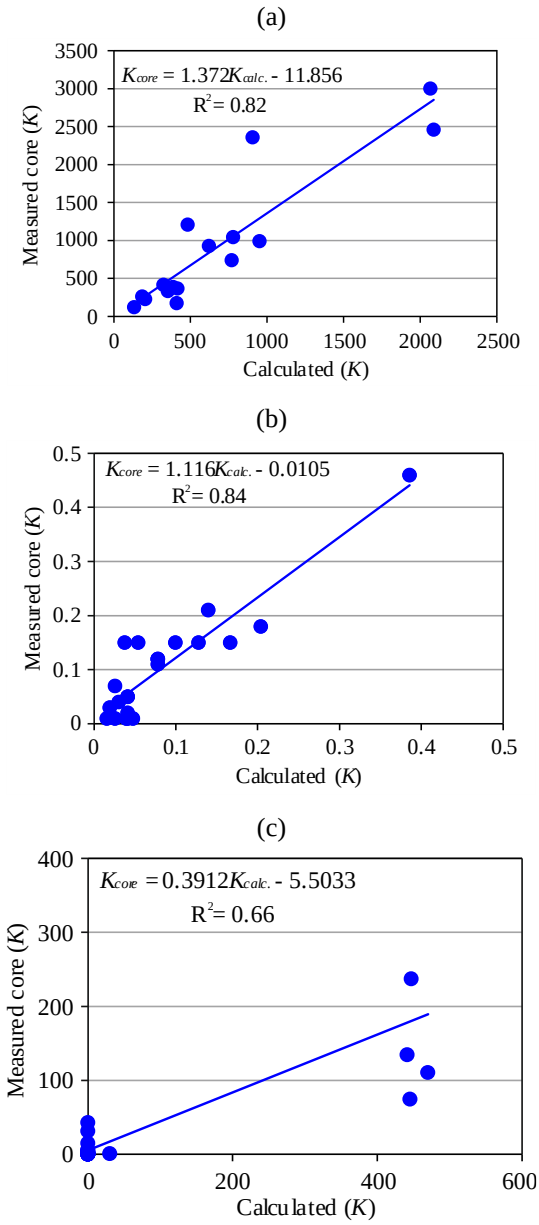

Figure 15. Measured core permeability and calculated permeability (K) validation for Matulla: (a) Muzhil-4 well (11541-11576); (b) Muzhil-7 well (12390-12434); (c) Muzhil-8 well (11396-11457)

The neutron-density log combination and resistivity log were used for the identification and characterization of various fluids in the reservoir zones. Based on visual observation of these logs, some selected reservoir zones were identified as hydrocarbon (oil) bearing zones. This is due to the detected neutron-density crossover and high resistivity values observed in some intervals and marked by yellow color, as shown in (Fig. 13a-e). Resistivity logs are commonly used to differentiate types of hydrocarbon fluids in the sense that liquid hydrocarbon normally displays higher resistivity values compared to gas zones. Based on these observations, the type of hydrocarbon fluid that could be found in these reservoirs is oil.

The measured porosity, permeability, and water saturation from core samples are plotted against the log-calculated porosity, permeability, and water saturation respectively Figures 14-16 and Table 4 in the cored intervals in Muzhil-4, Muzhil-7, and Muzhil-8 wells.

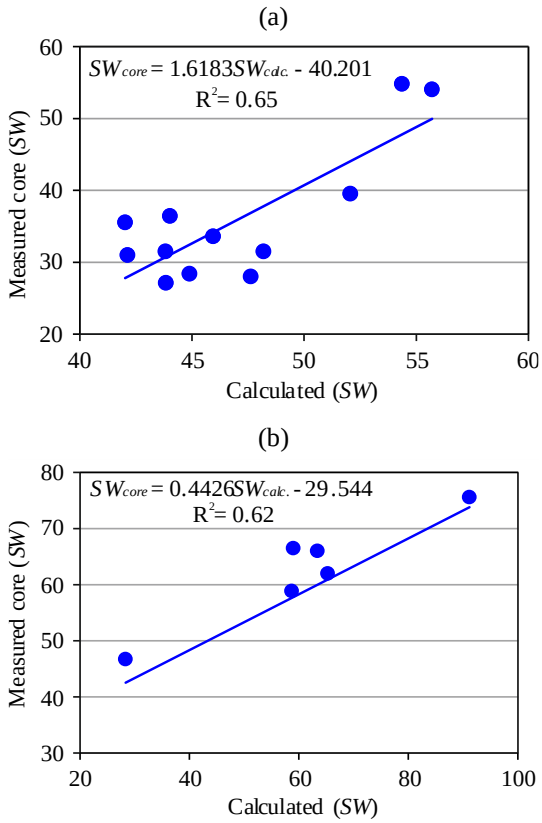

Figure 16. Measured core water saturation and calculated water saturation (S_w) validation for Matulla Formation: (a) Muzhil-4 well (11541-11579); (b) Muzhil-4 well (11580-11611)

The correlations show a fair to good degree of validation to be used for calculating similar petrophysical parameters in the other wells where no core samples are available.

4.3.3. Fluid contacts in Matulla Formation

One of the most important applications of petrophysical evaluations is the determination of hydrocarbon-water contacts. The measured pressure points were recorded in 4 wells only through the Matulla reservoir and have been plotted vs. depth (Fig. 17). The measured pressure quality, type of fluid and the calculated hydrostatic gradient are shown. The contacts for the Matulla reservoir in all wells were investigated individually.

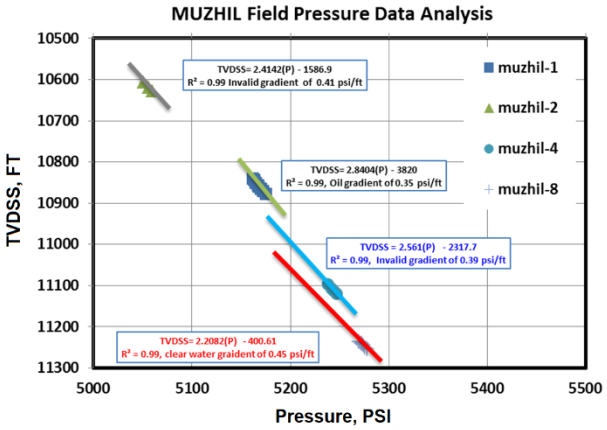

Figure 17. The measured pressure vs. depth in the Matulla reservoir, in all studied wells

Table 4. Correlation results between measured and calculated porosity, permeability and water saturation in cored intervals at Muzhil-4, Muzhil-7 and Muzhil-8 wells

Well	Equation		
	Porosity (Φ)	Permeability (K)	Water saturation (Sw)
Muzhil-4	$\Phi_{core} = 1.6997\ \Phi_{calc} - 10.569$ $R^2 = 0.63$	$K_{core} = 1.372\ K_{calc} - 11.856$ $R^2 = 0.82$	$Sw_{core} = 1.6183\ Sw_{calc} - 40.201$ $R^2 = 0.6548$
Muzhil-7	$\Phi_{core} = 1.0508\ \Phi_{calc} + 4.7579$ $R^2 = 0.75$	$K_{core} = 1.116\ K_{calc} + 0.0105$ $R^2 = 0.84$	$Sw_{core} = 0.4212\ Sw_{calc} + 39.696$ $R^2 = 0.68$
Muzhil-8	$\Phi_{core} = 0.7902\ \Phi_{calc} + 4.2809$ $R^2 = 0.83$	$K_{core} = 0.3912\ K_{calc} + 5.5033$ $R^2 = 0.66$	$Sw_{core} = 2.9532\ Sw_{calc} - 217.62$ $R^2 = 1$

The Free Water Level (FWL) was considered and compared against the S_{ws} on the logs. The fluid analysis results (oil-water contact (OWC), oil down to (ODT), and water up to (WUT)) of all the wells, Oil down to (ODT) is -11095, water up to (WUT) is -11233, and Oil-water contact (OWC) is non.

An initial oil down to the Matulla reservoir was assigned at -10955 ft, where as an initial up to Matulla reservoir was assigned at -11233 ft which could be identified from the well log analysis of Muzhil-1 and Muzhil-8 wells. While the other studied wells in the same level varied from water hole to Oil down to. Matulla Formation does not show a definite gas water or oil water contact based on the petrophysical evaluation of the studied wells.

The Matulla Formation is the most promising oil reservoir in the Muzhil field. Different pressure regimes were reported. Figure 17 shows that the pressure gradients in the Matulla Formation in Muzhil-1 and Muzhil-2 represent oil type, whereas those in Muzhil-7 and Muzhil-8 represent water production from the Matulla Formation.

4.3.4. Lateral variations of petrophysical characteristics

Lateral variation of petrophysical characteristics could be studied using constructed isoparametric maps. The study of these petrophysical parameter maps is very important in judging their lateral variation and the factors that control them, which may be either stratigraphic, structural, or both (Fig. 18a-f).

4.3.4.1. Shale content distribution

Shale content is an important quantitative function of log analysis. It is an important indicator of reservoir quality, in a lower V_{sh} usually reveals a better reservoir. Figure 18a represents the distribution of the shale content of the Matulla reservoir. It ranges from (21 and 40%). The shale content increases relatively towards the north part of theMuzhil-8 well and decreases towards the southeastern direction in Muzhil-1 well. In general, the Matulla reservoir facies have a high shale content, and the V_{sh} calculations suggested that the Matulla reservoir is shaly sandstone.

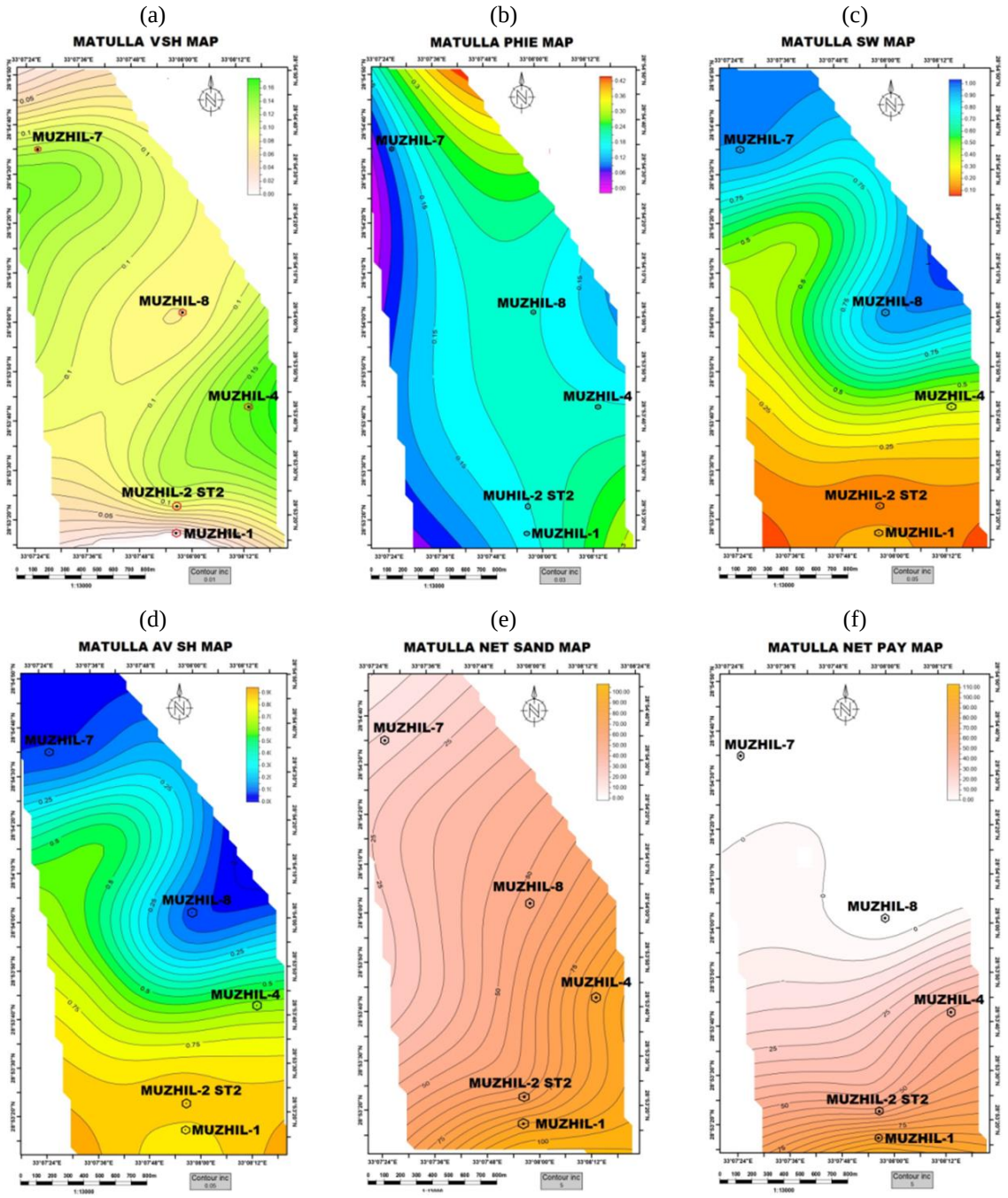

Figure 18. Isoparametric maps of Matulla sandstone: (a) the shale content; (b) the effective porosity; (c) water saturation; (d) hydrocarbon saturation; (e) Net Sand; (f) the net pay

4.3.4.2. Effective porosity distribution

The Φ_e is the most important petrophysical parameter in the evaluation of hydrocarbon potentiality. The structural element may affect the Φ development, which has a great influence on the Φ [77]. Figure 18c represents the distribution of the Φ_e of Matulla reservoir. It ranges from 15 and 19%. It increases in the northwestern direction at the Muzhil-7 well and decreases in the southwestern direction at Muzhil-1 and Muzhil-2 wells. The Φ_e has the maximum value in the northwestern part and the minimum value in the western part in Muzhil-1 and Muzhil-2 wells.

4.3.4.3. Water saturation distribution

Figure 18c represents the distribution of the water saturation of Matulla. It ranges from 20% as in both Muzhil-1 and Muzhil-2 to 100% as in both Muzhil-7 and Muzhil-8. It decreases in the southeastern direction at Muzhil-1 and Muzhil-2 wells and increases in the northeastern direction at the Muzhil-7 and Muzhil-8 wells. Generally, The S_w increases from southwest to northeast and east directions and decreases from east to west and southwest directions.

4.3.4.4. Hydrocarbon saturation distribution

The determination of hydrocarbon saturation is the main target of the current study. All maps show regional matching for hydrocarbon with S_w. Figure 18d represents distribution of the S_h of Matulla. It ranges from 0% as in both Muzhil-8 and Muzhil-7 to 80% as in Muzhil-2. It increases in the southeastern direction at Muzhil-1 and Muzhil-2 wells and decreases in the west direction at the Muzhil-7 and Muzhil-8 wells. Generally, it increases toward the southeastern part and decreases toward the northwestern part of the field.

4.3.4.5. Net sand distribution

The distribution of the net pay thickness is constructed to show the lateral variation of thickening and thinning of the effective thickness of the studied rock units. Figure 18e illustrates the effective thickness distribution of the Matulla reservoir zone. The sandstone effective thickness varies between 0 and 83 ft. The thickness increases toward the southeastern part in Muzhil-1, and Muzhil-2 wells and decreases toward the northwest part in Muzhil-7 well. This variation indicated that the sedimentation lope in Matulla starts from the southeast to the northwest direction.

The net sand map for the Matulla Reservoir (Fig. 18e) shows an overall decrease towards the west and north west while increasing towards the southeastern part of the study area. The minimum value is 16.5 ft at Muzhil-7 Well, while the maximum value attains (83 ft) at Muzhil-1 Well. The sand distribution map shows the extension of the sand to the East & South-East direction.

4.3.4.6. Net pay distribution

The distribution of the net pay thickness is constructed to show the lateral variation of thickening and thinning of the effective thickness of the studied rock units. Figure 18f illustrates the effective thickness distribution of the Matulla reservoir zone. The sandstone effective thickness varies between 0 and 83 ft. The thickness increases towards the southeastern part in Muzhil-1, and Muzhil-2 wells and decreases toward the northwest part in Muzhil-7 well. This variation indicated that the sedimentation slope in Matulla starts from the southeast to the northwest direction.

4.3.5. Hydrocarbon volume estimation in Matulla Formation

Hydrocarbon volumes are computed using parameters imputed into the static reservoir model, and the accuracy of volumetric depends on the integrity of Φ, saturation, net thickness, areal extent. and formation volume factor values. This estimation is very critical as the value determines whether or not the company proceeds with further exploration, and production activities in the field. Stock Tank Oil Initially in Place (STOIIP) is estimated using Formulas (21) and (22).

The calculation of the Original Oil in Place (OOIP) has been done only for the development segment of Muzhil Field. A B_o factor of 1.28 rb/stb was used, the pay thickness is 72, hydrocarbon saturation of 35, the porosity is 17, the area of 524 acres, and oil volume factors of 1.28, and therefore the result of the STOIIP in the Matulla reservoir is 13.609 MMBBL.

4.3.6. Recommendations

The deduced petrophysical characteristics results of the Late Cretaceous Matulla Formation reflect the ability of its sediments to host more promising reservoir intervals for storing and producing hydrocarbons, which should be considered during future exploration and development. Hydrocarbon production from the Muzhil oil field is expected from drilling wells, especially in the southeastern part of the studied area in the vicinity of Muzhil-1and Muzhil-2 wells due to the more favourable economic conditions. Avoiding drilling in areas of high Sw around Muzhil-7 and Muzhil-8 wells is also recommended.

5. Conclusions

The lithology of Matulla reservoir rock in all studied wells is composed mainly of sandstone with intercalations of shale and some limestone stricks. In general, structural and stratigraphic parameters control the lateral variation of the Matulla reservoir. The average volume of shale varies from (20-40%).The major type of clay mineral that existed in the Matulla Formation, as identified from Th-K, PEF-Th/K ratio, and PEF-K cross plots, is the montmorillonite which highly affects the porosity of the reservoir. Besides, the PEF has a wide range of values, reflecting a mixed nature of minerals. Clays are distributed in the sand, mainly in laminated and dispersed forms. Laminated clays induce a minimal effect on the pore volume; whereas dispersed shale significantly reduces the pore volume, but increases the S_w probably due to their elevated contents of irreducible S_w.

The determined reservoir characterization shows that the Matulla reservoir has an effective porosity value from 15 to 19% and the porosity type is mainly intergranular, particularly in the quartzose sandstones. The average V_{sh} is 21-40%, the average S_w of about 20 to 100%, the average S_{hc} is about 0 to 80%, and the net pay gets thicknesses from zero to 83 ft.The obtained S_h suggests that the Matulla sandstone in the study area contains hydrocarbon (oil) with commercial quantities. The total reservoir characterization shows an average Φ_e of about 16.6%, an average V_{sh} about 31.8%, an average S_w of about 66.4%, and an average S_{hc} of about 33.8%. The S_{hc} distribution of Matulla reservoir increases to the southern direction towards Muzhil-1 and Muzhil-2 wells and decreases to the north direction towards the Muzhil-7 and Muzhil-8 wells. The S_{hc} has the maximum value of 80% in Muzhil-2 well. The net pay thickness of Matulla reservoirs varies from 0 and 83 ft. It increases towards the south direction of the Muzhil-1 and Muzhil-2 wells and decreases to the western part towards Muzhil-7 and Muzhil-8 wells. The Matulla streaky sandstone facies increased towards the south part in Muzhil-1 and Muzhil-2 wells and decreases to the northern part, while it changed to blocky sandstone facies in Muzhil-1 well. There is a good quantity of oil in the Matulla reservoir; the calculated oil initially in place within the Matulla sandstone is equal to 1154963 stock tank barrels (13.609 MMBBL) in all the studied wells.

Acknowledgements

The authors wish to express their thanks and gratitude to the Egyptian General Petroleum Corporation (EGPC) and South Abu Zienima Company (SAZ) authority for permission and release of the data for this research.

References

[1] Robson, D.A. (1971). The structure of the Gulf of Suez (Clysmic) rift, with special reference to the eastern side. *Journal of the Geological Society*, *127*(3), 247-271. https://doi.org/10.1144/gsjgs.127.3.0247

[2] Bobbitt, J.E., & Gallagher, J.O. (1978). The petroleum geology of Ihe Gulf of Suez. *Offshore Technology Conference*, OTC-3091-MS https://doi.org/10.4043/3091-MS

[3] Rohrback, B.G. (1982). Crude oil geochemistry of the Gulf of Suez. *Exploration and Production Conference*, (1), 212-224.

[4] Shahin, A.N., & Shehab, M.M. (1984). Petroleum generation, migration and occurrences in the Gulf of Shore of South Sinai. *Proceeding of the 7th Petroleum Exploration Seminar*, 126-151.

[5] Alsharhan, A.S., & Salah, M.G. (1994). Geology and hydrocarbon habitat in rift setting: southern Gulf of Suez, Egypt. *Bulletin of Canadian Petroleum Geology*, *42*(3), 312-331.

[6] Patton, T.L., Moustafa, A.R., Nelson, R.A., & Abdine, S.A. (1994). Tectonic evolution and structural setting of the Suez rift. *American Association of Petroleum Geologists Memoir*, (59), 9-55. https://doi.org/10.1306/M59582C2

[7] EGPC. (1996). *Gulf of Suez Oil Fields (A comprehensive overview)*. Cairo, Egypt: Egyptian General Petroleum Corporation, 736 p.

[8] Barakat, A.O., Mostafa, A., El-Gayar, M.S., & Rullkotter, J. (1997). Source-dependent biomarker properties of five crude oils from the Gulf of Suez, Egypt. *Organic Geochemistry*, (26), 441-450. https://doi.org/10.1016/S0146-6380(97)00028-4

[9] Alsharhan, A.S. (2003). Petroleum geology and potential hydrocarbon plays in the Gulf of Suez rift basin, Egypt. *AAPG bulletin*, *87*(1), 143-180.

[10] Bosworth, W., & Mc Clay, K. (2001). Structural and stratigraphic evolution of the Gulf of Suez rift, Egypt: A synthesis. *Mémoires du Muséum National d'Histoire Naturelle*, (186), 567-606.

[11] Zalat, A.A., Zaid, S.M., Gadallah, M.H., & Abdel-Aziz, Z.A. (2012). Sandstones reservoir quality of the Matulla Formation, Gulf of Suez, Egypt. *Australian Journal of Basic and Applied Sciences*, *6*(12), 511-529.

[12] El-Sharawy, M.S., & Nabawy, B.S. (2015). Geological and petrophysical characterization of the lower Senonian Matulla Formation in Southern and Central Gulf of Suez, Egypt. *Arabian Journal for Science and Engineering*, (41), 281-300. https://doi.org/10.1007/s13369-015-1806-7

[13] Sarhan, M.A., Collier, R.E.L, Basal, A., & Aal, M.H.A. (2014). Late Miocene normal faulting beneath the northern Nile delta: NNW propagation of the Gulf of Suez Rift. *Arabian Journal of Geosciences*, *7*(11), 4563-4571. https://doi.org/10.1007/s12517-013-1089-9

[14] El-Sabbagh, A., Tantawy, A.A., Keller, G., Khozyem, H., Spangenberg, J., Adatte, T., & Gertsch, B. (2011). Stratigraphy of the Cenomanian-Turonian oceanic anoxic event OAE2 in shallow shelf sequences of NE Egypt. *Cretaceous Research*, *32*(6), 705-722. https://doi.org/10.1016/j.cretres.2011.04.006

[15] Kassem, A.A., Sharaf, L.M., Baghdady, A.R., & El-Naby, A.A. (2020). Cenomanian/Turonian oceanic anoxic event 2 in October oil field, Central Gulf of Suez, Egypt. *Journal of African Earth Sciences*, (165), 103817. https://doi.org/10.1016/j.jafrearsci.2020.103817

[16] Shehata, A.A., Kassem, A.A., Brooks, H.L., Zuchuat, V., & Radwan, A.E. (2021). Facies analysis and sequence-stratigraphic control on reservoir architecture: Example from mixed carbonate/siliciclastic sediments of Raha Formation, Gulf of Suez, Egypt. *Marine and Petroleum Geology*, (131), 105160. https://doi.org/10.1016/j.marpetgeo.2021.105160

[17] Said, R., (1961). Tectonic framework of Egypt and its influence on distribution of foraminifera. *AAPG Bulletin*, *45*(2), 198-218. https://doi.org/10.1306/0BDA6335-16BD-11D7-8645000102C1865D

[18] Said, R. (1963). Structural setting of gulf of Suez, Egypt. In *World Petroleum Congress* (pp. 1-8).

[19] Said, R. (1990) *Geology of Egypt*. London, United Kingdom: CRC Pres Balkema, 743 p. https://doi.org/10.1017/S0016756800019828

[20] Said, R. (2017). *The Geology of Egypt*. London, United Kingdom: Routledge, 734 p. https://doi.org/10.1201/9780203736678

[21] Mostafa, A.R. (1993). Organic geochemistry of source rocks and related crude oils in the Gulf of Suez, Egypt. *Geowissenschaften Abbandlungen*, (147), 163. https://doi.org/10.3997/2214-4609.201411824

[22] Mostafa, A.R., Klitzsch, E., Matheis, G., & Ganz, H., (1993). Origin and evaluation of hydrocarbons in the gulf of Suez Basin, Egypt. *Geoscientific Research in North East Africa*, 267-275. https://doi.org/10.1201/9780203753392-51

[23] Hassouba, A., Sarrawi, M., & Sakr, S. (1994). Early Syn-Rift sedimentation in October Field Area: A stratigraphic model for hydrocarbon accumulation. In *Petroleum Exploration and Production Conference* (pp. 341-350).

[24] Zein El Din, M.Y, Klitzsch, E., Abd El Hady, M.A., & Abd El Gawad, E.A. (1995). Evaluation of Kareem/Rudeis carbonate reservoir in Zeit Bay Field, Gulf of Suez, Egypt. *Science and Development*, 20-30.

[25] McClay, K.R., Nichols, G.J., Khalil, S.M., Darwish, M., & Bosworth, W. (1998). Extensional tectonics and sedimentation, eastern Gulf of Suez, Egypt. *Sedimentation and Tectonics in Rift Basins Red Sea: Gulf of Aden*, 223-238. https://doi.org/10.1007/978-94-011-4930-3_14

[26] Winn, R.D.Jr., Crevello, P.D., & Bosworth, W. (2001). Lower Miocene Nukhul formation, Gebel el Zeit, Egypt: model for structural control on early Sunrift strata and reservoirs, Gulf of Suez. *AAPG Bulletin*, *85*(10), 1871-1890. https://doi.org/10.1306/8626D095-173B-11D7-8645000102C1865D

[27] Guiraud, R., Bosworth, W., Thierry, J., & Delplanque, A. (2005). Phanerozoic geological evolution of northern and central Africa: An overview. *Journal of African Earth Sciences*, *43*(1-3), 83-143. https://doi.org/10.1016/j.jafrearsci.2005.07.017

[28] El-Azabi, M.H., & El-Araby, A. (2007). Depositional framework and sequence stratigraphic aspects of the Coniacian-Santonian mixed siliciclastic/carbonate Matulla sediments in Nezzazat and Ekma blocks, Gulf of Suez, Egypt. *Journal of African Earth Sciences*, (47), 179-202. https://doi.org/10.1016/j.jafrearsci.2007.02.002

[29] Omran, M.A., & El Sharawy, M.S. (2014). Tectonic evolution of the Southern Gulf of Suez, Egypt: a comparison between depocenter and near peripheral basins. *Arabian Journal of Geosciences*, (7), 87-107.

[30] El Nady, M.M., Ramadan, F.S., Hammad, M.M., & Lotfy, N.M. (2015). Evaluation of organic matters, hydrocarbon potential and thermal maturity of source rocks based on geochemical and statistical methods: Case study of source rocks in Ras Gharib oilfield, central Gulf of Suez. *Egyptian Journal of Petroleum*, *24*(2), 203-211. https://doi.org/10.1016/j.ejpe.2015.05.012

[31] Moustafa, A.R, & Khalil, S.M. (2020). Structural setting and tectonic evolution of the Gulf of Suez, NW Red Sea and Gulf of Aqaba Rift Systems. *The Geology of Egypt*, 295-342. https://doi.org/10.1007/978-3-030-15265-9_8

[32] Radwan, A.E., Trippetta, F., Kassem, A.A., & Kania, M. (2022). Multi-scale characterization of unconventional tight carbonate reservoir: Insights from October oil field, Gulf of Suez rift basin, Egypt. *Journal of Petroleum Science and Engineering*, (197), 107968. https://doi.org/10.1016/j.petrol.2020.107968

[33] Nabawy, B.S., Elgendy, N.T.H., & Gazia, M.T. (2020). Mineralogic and diagenetic controls on reservoir quality of Paleozoic Sandstones, Gebel El-Zeit, North Eastern Desert, Egypt. *Natural Resources Research*, (29), 1215-1238. https://doi.org/10.1007/s11053-019-09487

[34] Chowdhary, L.R., & Taha, S. (1987) Geology and habitat of oil in Ras Budran field, Gulf of Suez. *AAPG Bulletin*, *71*(10), 1274-1293. https://doi.org/10.1306/9488703C-1704-11D7-8645000102C1865D

[35] Barakat, M.G., Darwish, M., & El Outefi, N.S. (1988). Eocene tectonostratigraphy and basin evaluation in the Gulf of Suez petroliferous province. *Proceedings of the 9th Egyptian General Petroleum Corporation, Petroleum Exploration and Production Conference, Cairo, Egypt*, (1), 1-22.

[36] Schlumberger. (1984). Geology of Egypt. *Well Evaluation Conference*, 1-64.

[37] Nabeel, H., Gawad, E., Hammed, M., & Naggar, H. (2016) Subsurface structural imaging and architecture of pre-rift sediments of west Hurghada district. *International Journal of Innovative Science, Engineering & Technology*, *3*(12), 84-98.

[38] Atta, M.A., Shahin, A.N., Blanchard, D., & David, H. (2002). Petroleum potential of the Gemsa Basin, southern Gulf of Suez, Egypt. *International Petroleum Conference and Exhibition*, 27-30.

[39] Peijs, J.A., Bevan, T.G., & Piombino, J.T. (2012). The Gulf of Suez rift basin. *Regional Geology and Tectonics: Phanerozoic Rift Systems and Sedimentary Basins*, 165-194. https://doi.org/10.1016/B978-0-444-56356-9.00007-9

[40] Schutz, K. (1994). Structure and stratigraphy of the Gulf of Suez, Egypt. *Interior Rift Basins*, (59), 1-14. https://doi.org/10.1306/M59582C3

[41] El Diasty, W.S., & Peters, K.E. (2014). Genetic classification of oil families in the central and southern sectors of the Gulf of Suez, Egypt. *Journal of Petroleum Geology*, *37*(2), 105-126. https://doi.org/10.1111/jpg.12573

[42] Abulkaramat, S., & Meshref, W. (2002). Reverse fault geometry in the Gulf of Suez Rift Basin, Egypt. *International Petroleum Conference and Exhibition*, 27-30.

[43] Abd-Allah, AM, Aal, M.H.A, El-Said, M.M., & El-Naby, A.A. (2014). Structural evolution of the southern transfer zone of the Gulf of Suez rift. *Journal of African Earth Sciences*, (96), 21-38. https://doi.org/10.1016/j.jafrearsci.2014.03.008

[44] Khalil, S.M., & McClay, K.R. (2001). Tectonic evolution of the NW Red Sea-Gulf of Suez rift system. *Geological Society, London, Special Publications*, *187*(1), 453-473. https://doi.org/10.1144/GSL.SP.2001.187.01.22

[45] Tamsett, D. (1984). Comments on the development of rifts and transform faults during continental breakup; examples from the Gulf of Aden and northern Red Sea. *Tectonophysics*, (104), 35-46. https://doi.org/10.1016/0040-1951(84)90100-8

[46] Feinstein, S., Kohn, B.P., Steckler, M.S, & Eyal, M. (1996). Thermal history of the eastern margin of the Gulf of Suez, I. reconstruction from borehole temperature and organic maturity measurement. *Tectonophysics*, *266*(1-4), 203-220. https://doi.org/10.1016/S0040-1951(96)00190-4

[47] Marttila, R.K., & El Bahr, M., (1994). Evaluation of a lithology complex reservoir (Nezzazat Group) in the Gulf of Suez. *12th EGPC Exploration and Production Conference*, (2), 472-482.

[48] Said, S.G., Faris, M., Zalat, A., & Soliman, A. (2022). Palynological studies on the Upper Cretaceous Wata and Matulla Formations in Bakr Oil Field, Gulf of Suez, Egypt. *Delta Journal of Science*, *44*(1), 81-98. https://doi.org/10.21608/djs.2022.114256.1009

[49] Zahra, H.S., & Nakhla, A.M. (2015). Deducing the subsurface geological conditions and structural framework of the NE Gulf of Suez area, using 2-D and 3-D seismic data. *NRIAG Journal of Astronomy and Geophysics*, *4*(1), 64-85. https://doi.org/10.1016/j.nrjag.2015.04.003

[50] Schlumberger. (2015). *Techlog Wellbore Software Platform version 2015.1*. Retrieved from: www.software.slb.com
[51] Asquith, G., & Gibson, C. (1982) *Basic well log analysis for geologists*. Tulsa, United States: American Association of Petroleum Geologists. https://doi.org/10.1306/Mth3425
[52] Rider, M. (1986). *The geological interpretation of well logs* (pp. 151-165). Blackie, Glasgow.
[53] Omran, A.A. (2000). Well log analysis and hydrocarbon potentialities of the Nukhul Formation in the northern part of the Gulf of Suez, Egypt. *5th International Symposium on the Geology of Arab States*, (31), 1-32.
[54] Omran, A.A., & Al Areeq, N.M. (2007). Reservoir characteristics and oil potentiality of the Upper Qishn Clastic Member, Masila Basin, Yemen. *International Conference on Geology of Tethys*, (1), 1-14.
[55] Omran, A.A., & Alareeq, N.M. (2014). Log-derived petrophysical characteristics and oil potentiality of the Upper Qishn Clastic Member, Masila Basin, Yemen. *Arabian Journal of Geosciences*, (7), 1733-1748. https://doi.org/10.1007/s12517-013-0871-z
[56] Al-Areeq, N.M., Abu El Ata, A.S., Maky, A.F., & Omran, A.A. (2011). Hydrocarbon potentialities of some upper Jurassic rock units in Masila block, Sayun-Masila Basin, Yemen. *Journal of Applied Geophysics*, *10*(2), 147-168.
[57] Chilingar, G.V. (1964). Relationship between porosity, permeability, and grain-size distribution of sands and sandstones. *Developments in sedimentology*, (1), 71-75.
[58] Asquith, G.B. (1985) *Handbook of log evaluation techniques for carbonate reservoirs*. Tulsa, United States: American Association of Petroleum Geologists. https://doi.org/10.1306/Mth5446
[59] Wyllie, M.R.J. (1963). *The fundamentals of well log interpretation*. New York, United States: Academic Press, 238 p.
[60] Burke, J.A., Campbell, R.L., & Schmidt, A.W. (1969). The litho Φ cross plots. *10th Anniversary Scientific Symposium*, 1-29.
[61] Doveton, H.J. (1996). *Log analysis of subsurface geology, concepts and computer methods*. New York, United States: John Wiley, 273 p.
[62] Schlumberger. (1972). *Log interpretation/charts*. Houston, United States: Schlumberger Well Services Inc.
[63] Bassiouni, Z. (1994) Theory, measurement and interpretation of well logs. *Textbook Series, Society of Petroleum Engineers*, (4). https://doi.org/10.2118/9781555630560
[64] Hameed, A.T., Aldabaj, A.A., & Ramadhan, A.A. (2019). Identifying hydrocarbon and shaly zones of Mishrif Formation in Nasiriya Oil Field by using well logs. *IOP Conference Series: Materials Science and Engineering*, *579*(1), 012033. https://doi.org/10.1088/1757-899X/579/1/012033
[65] Klaja, J., & Dudek, L. (2016). Geological interpretation of spectral gamma ray (SGR) logging in selected boreholes. *Nafta-Gaz*, *72*(1), 3-14. https://doi.org/10.18668/NG2016.01.01
[66] Schlumberger. (2003). *Geophysical Logging Report, Well R-20*. Schlumberger water services report submitted to LANI.
[67] Thomas, E., & Stieber, S. (1975). The distribution of shale in sandstones and its effect upon porosity. *SPWLA Annual Logging Symposium*, 4-7.
[68] Dresser Atlas. (1979). *Log Interpretation Charts. Dresser Atlas Division, Dresser Industries*. Houston, United States.
[69] Parra, R. (2001). *Basic petroleum geology and log analysis*. Houston, United States: Halliburton, 87 p.
[70] Poupon, A., & Leveaux, J. (1971). Evaluation of Sw in shaly formations. *SPWLA Annual Logging Symposium*, 1-13.
[71] Arps, J.J. (1953). The effect of temperature on the density and electrical resistivity of sodium chloride solutions. *Journal of Petroleum Technology*, *5*(10), 17-20. https://doi.org/10.2118/953327-G
[72] Buckles, R.S. (1965). Correlating and averaging connate Sw data. *Journal of Canadian Petroleum Technology*, *4*(1), 42-52. https://doi.org/10.2118/65-01-07
[73] Kuang, Li-C. (2005). *Application of wireline formation testing data*. Beijing, China: Petroleum Industry Press.
[74] Liu, N.-Q. (2005). *Practical interpretation method of modern well testing*. Beijing, China: Petroleum Industry Press.
[75] Mohamed, A.S., Mohamed, M.T., Omran, A.A., & Nabawy, B.S. (2023). Managing the risk of wellbore instability using geomechanical modeling and wellbore stability analysis for muzhil shale formation in Gulf of Suez, Egypt. *Journal of Engineering Sciences*, (4), 12-23. https://doi.org/10.21608/jesaun.2023.201902.1215
[76] Selley, R.C., & Sonnenberg, S.A. (2014). *Elements of petroleum geology*. San Diego, United States: Academic Press, 528 p.
[77] El kadi Abderrezzak, K., & Paquier, A. (2009). One-dimensional numerical modeling of sediment transport and bed deformation in open channels. *Water Resources Research*, *45*(5). https://doi.org/10.1029/2008WR007134.

Петрофізичний аналіз та потенціал вуглеводнів пласта Матулла на родовищі Мужил, центральна частина Суецької затоки, Єгипет

А.С. Мохамед, А.А. Омран, М.Т. Мохамед, Б.С. Набави

Мета. Дослідження та оцінка петрофізичних характеристик пізньокрейдяного віку пласта Матулла в центральній частині Суецької затоки для виявлення потенціалу її вуглеводневого покладу.

Методика. Для оцінки покладів Матуллана основі комп'ютеризованого підходу було використано каротажні дослідження п'яти свердловин (Мужил-1, -2, -4, -7, -8). Петрофізичні параметри та типи флюїдів були розраховані, перевірені за керновими даними та представлені вертикально у вигляді крос-щілин літозасиченості та по латералі у вигляді карт ізопараметричних варіацій.

Результати. Надано оцінку загальної пористості (Φ_t), ефективної пористості (Φ_e), вмісту глинистих сланців (V_{sh}), водонасиченості (S_w), проникності (K), загального об'єму води (BVW) і чистих продуктивних характеристик пласта Матулла в свердловинах Мужил, що показує наступні середньозважені значення: 18-23%, 15-19%, 21-40%, 20-100%, 1.1-281 mD, 3-21% та 0-83 ft відповідно. Визначено на основі ідентифікації літології, отриманої за даними каротажу, що основним матричним компонентом пласта Матулла є кварцовий пісковик з незначним вмістом сланцю та карбонату. Зазначено, що верхня зона є поганим покладом, тоді як середня та нижня зони вважаються досить хорошими покладами у всіх досліджуваних свердловинах. Очікується, що Мужил-2 видобуватиме нафту без використання води; але Мужил-1 і Мужил-4 видобуватимуть нафту з водою; в той час як Мужил-7 і Мужил-8 виробляти муть тільки воду.

Наукова новизна. Надано детальну петрофізичну оцінку за допомогою каротажу, підтверджену аналізом керна та випробуваннями свердловин (DST і MDT), а побудова крос-щілин літозасиченості для кожної свердловини та ізопараметричних петрофізичних карт виконані вперше для пласта Матулла родовища Мужил.

Практична значимість. Отримані результати з літозасиченості та петрофізики розширили знання про характеристики відкладень пласта Матулла, вміщуючих перспективні інтервали покладів, і мають бути враховані при подальших дослідженнях та розробці родовища Мужил.

Ключові слова: *потенціал вуглеводнів, каротаж свердловин, оцінка пласта, петрофізичні параметри, пласт Матулла, родовище Мужил, Суецька затока*